DRH

OUTER SATELLITE ATMOSPHERES: THEIR NATURE AND PLANETARY INTERACTIONS

Final Report for Period February 1979 to March 1980

prepared for
NASA HEADQUARTERS
WASHINGTON, D.C. 20546

prepared by
William H. Smyth

ATMOSPHERIC AND ENVIRONMENTAL RESEARCH, INC.
872 Massachusetts Avenue Cambridge, Massachusetts 02139

TECHNICAL REPORT STANDARD TITLE PAGE

1. Report No.	2. Government Accession No.	3. Recipient's Catalog No
Seven		

4. Title and Subtitle	5. Report Date
Outer Satellite Atmospheres: Their Extended Nature and Planetary Interactions	April 1980
	6. Performing Organization Code

7. Author(s)	8. Performing Organization Report No
William H. Smyth	

9. Performing Organization Name and Address	10. Work Unit No.
Atmospheric and Environmental Research, Inc. 872 Massachusetts Avenue Cambridge, Massachusetts 02139	11. Contract or Grant No. NASW-3174
	13. Type of Report and Period Covered Final Report
12. Sponsoring Agency Name and Address NASA Headquarters Headquarters Contract Division Washington, DC 20546	14. Sponsoring Agency Code HW-2

15. Supplementary Notes

16. Abstract

Highly developed numerical models are applied to interpret extended-atmosphere data for the sodium cloud of Io and the hydrogen torus of Titan. Solar radiation pressure was identified and verified by model calculations as the mechanism to explain two different east-west asymmetries observed in the sodium cloud. Analysis of sodium line profile data, suggesting that a Jupiter magnetospheric wind may be responsible for high speed sodium atoms emitted form Io, and preliminary modeling of the interaction of the Io plasma torus and Io's sodium cloud are also reported. Models presented for Titan's hydrogen torus are consistent both with the recent Pioneer 11 measurements and earlier earth-orbiting observations by the Copernicus satellite. A new research effort - developing models for extended gas and dust atmospheres of comets - was initiated and progress to date is reported.

17. Key Words (Selected by Author(s))	18. Distribution Statement
satellite atmospheres planetary magnetospheres comets	

19. Security Classif. (of this report)	20. Security Classif. (of this page)	21. No. of Pages	22. Price*
Unclassified	Unclassified	103	

*For sale by the Clearinghouse for Federal Scientific and Technical Information, Springfield, Virginia 22151.

PREFACE

Interpretation of extended-atmosphere data for the sodium cloud of Io and the hydrogen torus of Titan is performed using highly developed numerical models. The construction of a model to interpret data for dust and gaseous atmospheres of comets has also been undertaken. Of particular importance in the Io related modeling have been the discovery and model verification of solar radiation pressure as the mechanism to explain certain east-west asymmetries observed in the sodium cloud. Other sodium modeling has placed emphasis upon understanding the sodium line profile data and the interaction of the sodium cloud with the newly discovered hot Io plasma torus. For Titan, updated models of its hydrogen torus are presented and are in agreement with both earth-orbiting measurements of the Copernicus satellite and the more recent data acquired by the Pioneer 11 spacecraft.

The successful modeling of the Io sodium data provides a valuable framework for understanding the local atmosphere of the satellite and its influence and interrelation with the Jovian magnetosphere, particularly with the Io plasma torus. The models for Titan provide a similar framework for the Saturn system, which will increase in importance as the Voyager 1 spacecraft encounters the planet later this year. Cometary modeling, under development, will upon completion provide a support base for the NASA mission to Halley.

Results from modeling sodium data, in addition to the discovery of the solar radiation pressure mechanism, have been obtained through line profile studies. These studies suggest that the relative motion of the planetary magnetosphere past Io may provide a Jovian magnetospheric wind mechanism for escape of high speed sodium atoms from the local satellite atmosphere. Comparisons of ground-based sodium data and Voyager 1 plasma torus data have shown promise, upon further analysis, of providing useful constraints for the plasma and energy balance mechanisms in the torus. Model results for Titan show that the hydrogen torus is complete and has a Lyman-α intensity near the elongation points of the satellite orbit of order 200 Rayleighs. Such a torus should be easily detected by the UV instrument aboard the Voyager spacecrafts.

TABLE OF CONTENTS

LIST OF FIGURES

CHAPTER I

INTRODUCTION

Interest in understanding the atmospheres of the outer satellites, their extended nature and their planetary interactions, has grown significantly in the last decade. Major contributions have been made by both earth-based astronomy and spacecraft measurements. In 1979, the encounters of Voyager 1 and Voyager 2 spacecrafts with Jupiter provided a vast new source of data for the Galilean satellites, while the encounter of the Pioneer 11 spacecraft with Saturn obtained new and important information for Titan. Future encounters of Voyager with Saturn, the visit to Jupiter of the Galileo spacecraft, and strong earth-based observational programs will continue to provide fresh data and new insights.

Research efforts reported summarize results of our second year of modeling the extended atmospheres of the outer satellites. Modeling emphasis this year has been focused primarily upon understanding and interpretation of (1) data characterizing the extended sodium atmosphere of Io and its interactions with the Jovian magnetosphere and (2) data describing the extended hydrogen atmosphere of Titan. New results from Voyager and Pioneer 11 have been incorporated. In addition to this, a new comet research effort has been initiated. The first phase of developing models for interpretative analysis of the extended dust and gaseous atmospheres of comets has been completed and the second phase is currently in progress.

This past year, spacecraft explorations coordinated with ground-based observations have been of particular importance in advancing our knowledge of the atmosphere and the magnetospheric environment of the Galilean satellite Io. Noteworthy are the continued earth-based observational programs for both the sodium cloud and the S^+ cold Io plasma torus, and the Voyager spacecraft discovery of a new hot Io plasma torus centered on the satellite orbit. In addition, both earth-orbiting Copernicus satellite and Pioneer 11 spacecraft measurements of the extended hydrogen atmosphere of Titan have been reported.

With regard to Io's sodium cloud, the major modeling advance this year has been the discovery of solar radiation pressure as the mechanism responsible for certain east-west asymmetries in the cloud. These asymmetries are observed when cloud images are compared for diametrically opposite satellite phase angles east and west of Jupiter. This subject is discussed in Chapter II. Preliminary investigation and interpretation of the line profile data for the sodium cloud D-line emission and initial modeling of the interactions of the hot plasma torus and the sodium cloud were also pursued this year. Results are presented respectively in Chapter III and Chapter IV.

Models for the extended hydrogen torus of Titan, reported last year, have been updated to reflect more recently acquired knowledge. Both the new Pioneer 11 data and the older earth-orbiting measurements by the Copernicus satellite have been

incorporated. These two data bases appear to be consistent and modeling results are presented in Chapter V.

Understanding the dust and gaseous atmospheres of comets is a new research topic initiated the second half of this reporting year. This effort represents a natural extension of our previous modeling program for extended satellite atmospheres, since the dust and neutral gas atmospheres of comets may be treated in similar fashion. Progress in model development is discussed in Chapter VI.

A summary of the key modeling results of each chapter is presented in Chapter VII. A discussion of the direction and emphasis of future research is also included in Chapter VII and completes the report.

CHAPTER II

IO'S SODIUM CLOUD: EAST-WEST ASYMMETRIES

2.1 Introduction

In this chapter attention will be restricted to refining our current understanding of data describing the spatial distribution of the sodium cloud as a function of the satellite phase angle. The primary emphasis will be to provide an explanation for certain asymmetries observed in the cloud when data are compared for diametrically opposite satellite phase angles east and west of Jupiter. The spatial structure of the cloud is determined by studying and modeling Earth-based observations of the solar resonance scattered emission of sodium atoms in the D-lines.

Previous studies and modeling efforts (Matson et al., 1978; Smyth and McElroy, 1978) of spatial cloud data (Matson et al., 1978; Murcray and Goody, 1978) have shown that the dominant sodium D-line emission surrounds and precedes Io in its orbit, forming an incomplete torus, approximately one-quarter of the way around Jupiter. The most complete study was performed by Smyth and McElroy (1978). They concluded that the forward sodium cloud was aligned along a central axis in the orbit plane tilted approximately 35° toward Jupiter with respect to the line drawn through Io and tangent to the satellite orbit, that the sodium appeared to be ejected primarily from the inner hemisphere of the satellite with a mean velocity of 2.6 km sec^{-1} and with an emission source

strength of 2×10^{25} atoms sec^{-1}, and that the mean lifetime of sodium cloud atoms in the Jovian magnetosphere was between 15 and 20 hours. An illustration taken from their paper showing this orientation of the sodium cloud is given in Figure 1.

These earlier modeling results indicate that the global spatial features of the sodium cloud may, to a first approximation, be treated as a steady state cloud. Variations in the intensity pattern of the cloud with satellite phase angle seen on the sky plane are therefore largely due to the changing geometric viewing perspective of the Earth-observer. Small changes in the intensity of the cloud, occurring in a time of order 2 hours (Trafton, 1977; Murcray and Goody, 1978), presumably represent fluctuations in magnetospheric conditions that modulate the local ionizaton lifetime of the sodium atoms in the steady state cloud. Other changes observed in absolute intensity (Bergstralh et al., 1975; Bergstralh et al., 1977) and more recently in the spatial distribution Goldberg et al., 1978), when data are compared for satellite orbital phase angles separated by 180°, suggest however that the steady state picture of the cloud is not complete. These types of changes are referred to as the east-west asymmetries of the sodium cloud and imply that a time varying mechanism is operative with a period equal to the satellite period.

During our research efforts earlier this reporting year, solar radiation pressure was identified as a mechanism to explain the east-west asymmetries of the sodium cloud. The announcement of the discovery and preliminary supporting orbit

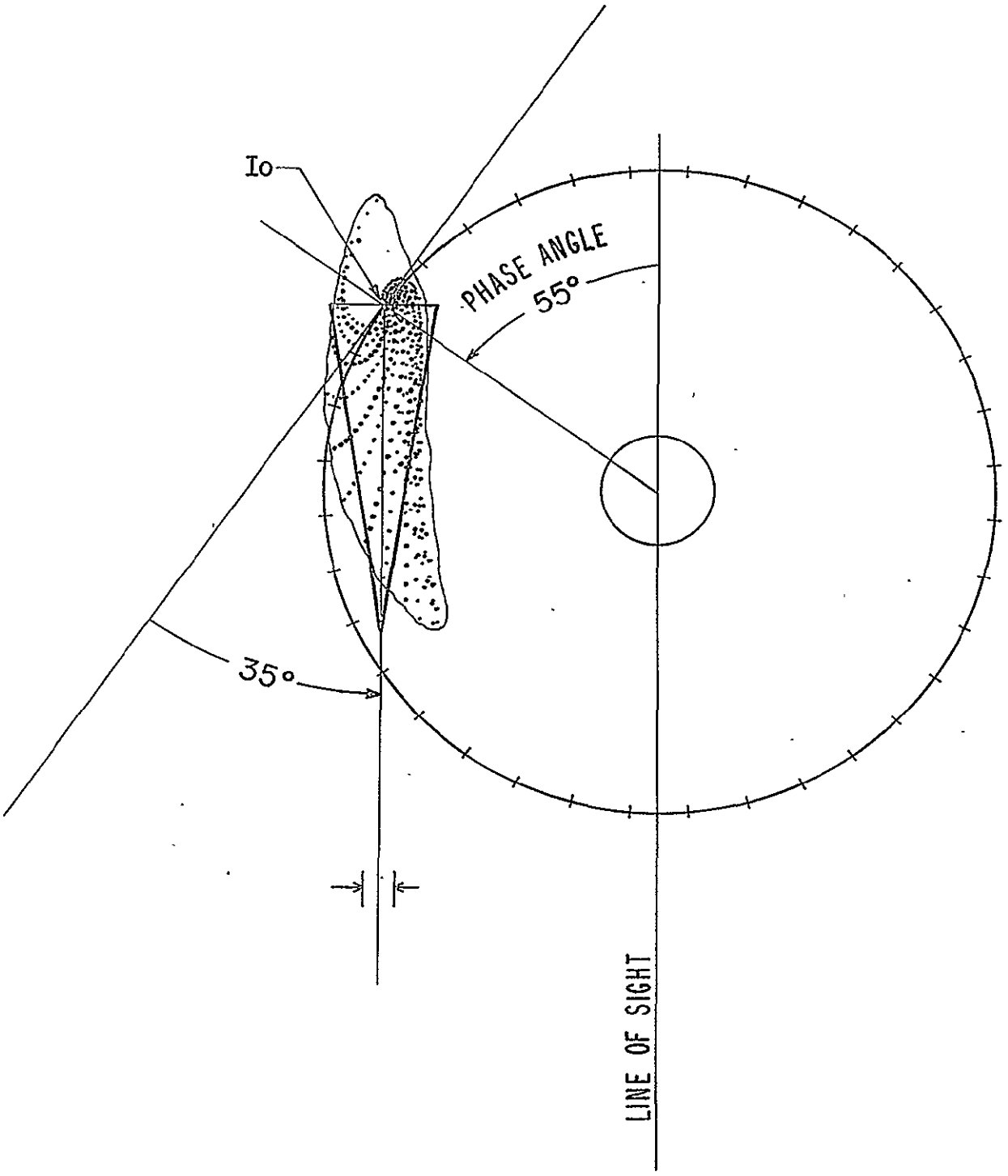

Figure 1. Sodium Cloud Model. The sodium cloud shape in the satellite plane calculated by Smyth and McElroy (1978), where density of points is proportional to atom concentration, is compared with their simple triangular model. An emission velocity of 2.6 km sec^{-1} and a lifetime of 20 hours were assumed.

calculations were published (Smyth, 1979) and are included in the Appendix. The preliminary calculations indicate that solar radiation pressure may explain both the east-west cloud intensity asymmetry of Bergstralh et al. (1975, 1977) and the intensity distribution asymmetry of Goldberg et al. (1978). To further test this hypothesis, the three-dimensional sodium cloud model has been modified to include the inherent time dependent effects of solar radiation pressure on the cloud atom orbits. Model calculations including the effects are reported here and verify the earlier preliminary conclusions. To provide background information for the more complete computations reported below, a brief review of the east-west asymmetry data and the preliminary analysis is in order.

Preliminary calculations in Figure 2 show the envelope of the sodium cloud both with and without the effect of solar radiation pressure, for diametrically opposite satellite phase angles of 55 degrees and 235 degrees. One obvious effect of the solar radiation pressure is to tilt the forward portion of the cloud closer to Jupiter when Io is near western elongation (270 degrees) than when Io is near eastern elongation (90 degrees). This behavior in the sodium cloud was observed by Goldberg et al. (1978). Their measurements indicate that the critical satellite phase angle along which the forward cloud axis is viewed to be approximately parallel to the observer's line of sight (so that the cloud appears relatively symmetric about Io) occurs at 65 degrees (Goldberg et al., 1978) to 70 or 75 degrees (Goldberg, 1979) in the east and

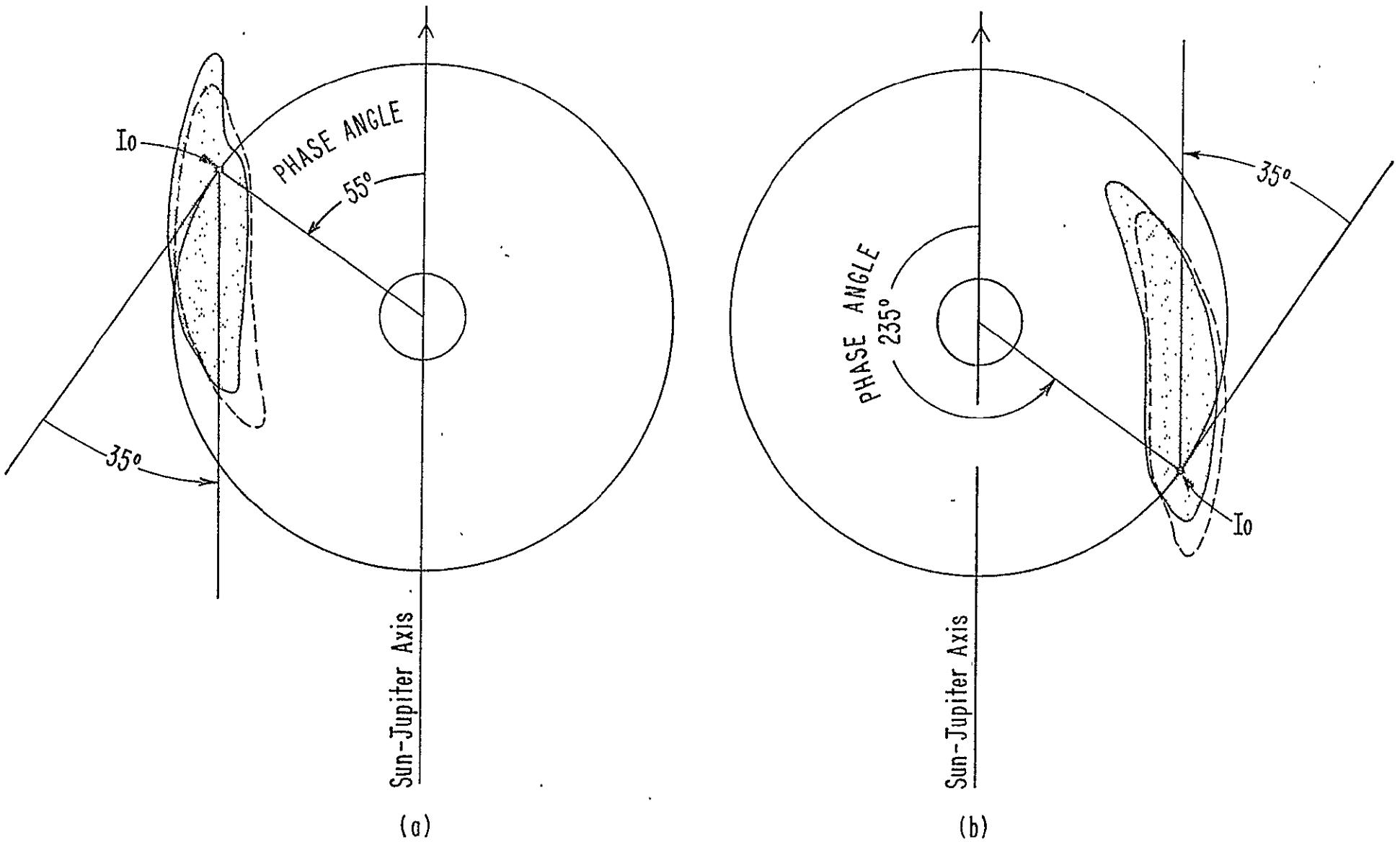

Figure 2. East-West Changes in the Sodium Cloud. The solar radiation perturbed cloud shape, indicated by the shaded area, and the unperturbed cloud shape, indicated by the dashed line, are compared for diametrically opposite phase angles.

230 degrees (Goldberg et al., 1978) in the west. In the east the central axis of the sodium cloud is therefore tilted only about 15 to 25 degrees with respect to the line drawn tangent to the satellite orbit at Io, whereas in the west the tilt angle is about 40 degrees. Thus, both the observations and model results of Figure 2 indicate a modulation of the tilt angle of the central cloud axis about the steady state central cloud axis location depicted in Figure 2.

The preliminary calculations in Figure 2 also indicate that solar radiation pressure causes the sodium cloud to be compressed near eastern elongation (90°) and to be expanded near western elongation. Measurements consistent with this behavior were reported by Bergstralh et al. (1975, 1978). They observed the intensity of the sodium cloud as a function of satellite phase angle through a 3 x 8 arc sec slit centered on the satellite as depicted in Figure 3 and concluded over a two year baseline that the measured intensity near eastern elongation was 20-25% brighter than the intensity near western elongation. Figure 4 shows the data published in the first of their two articles (Bergstralh et al., 1975), for which the reported intensity asymmetry is closer to 50%.

2.2 Model Results: Goldberg's Phase Lag Asymmetry

Observations of Goldberg et al. (1978) and Goldberg (1979) indicate that the projected intensity patterns of the sodium cloud on the plane of the sky do not produce mirror images at orbital phase angles separated by 180 degrees. Their measure-

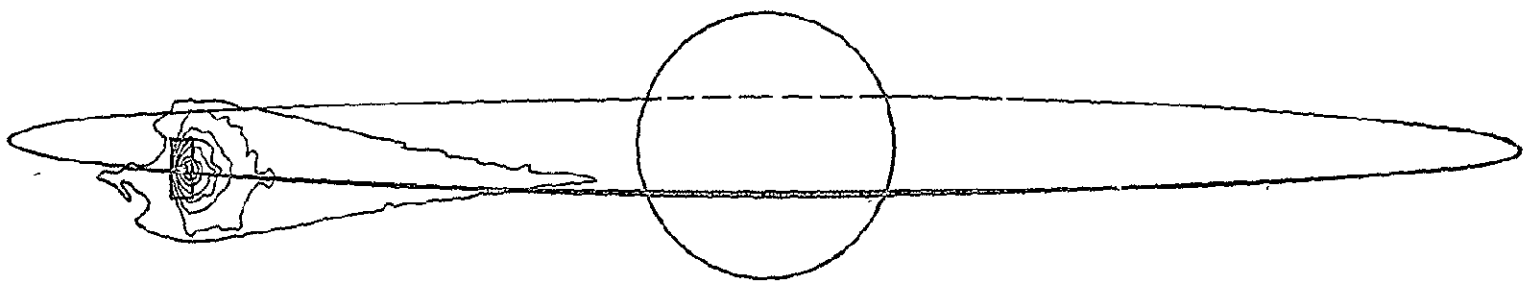

Figure 3. Observational Slit. The rectangular observational slit of Bergstralh et al. (1975, 1977), centered on Io, is shown in relationship to the sodium cloud, the satellite orbit and the planet.

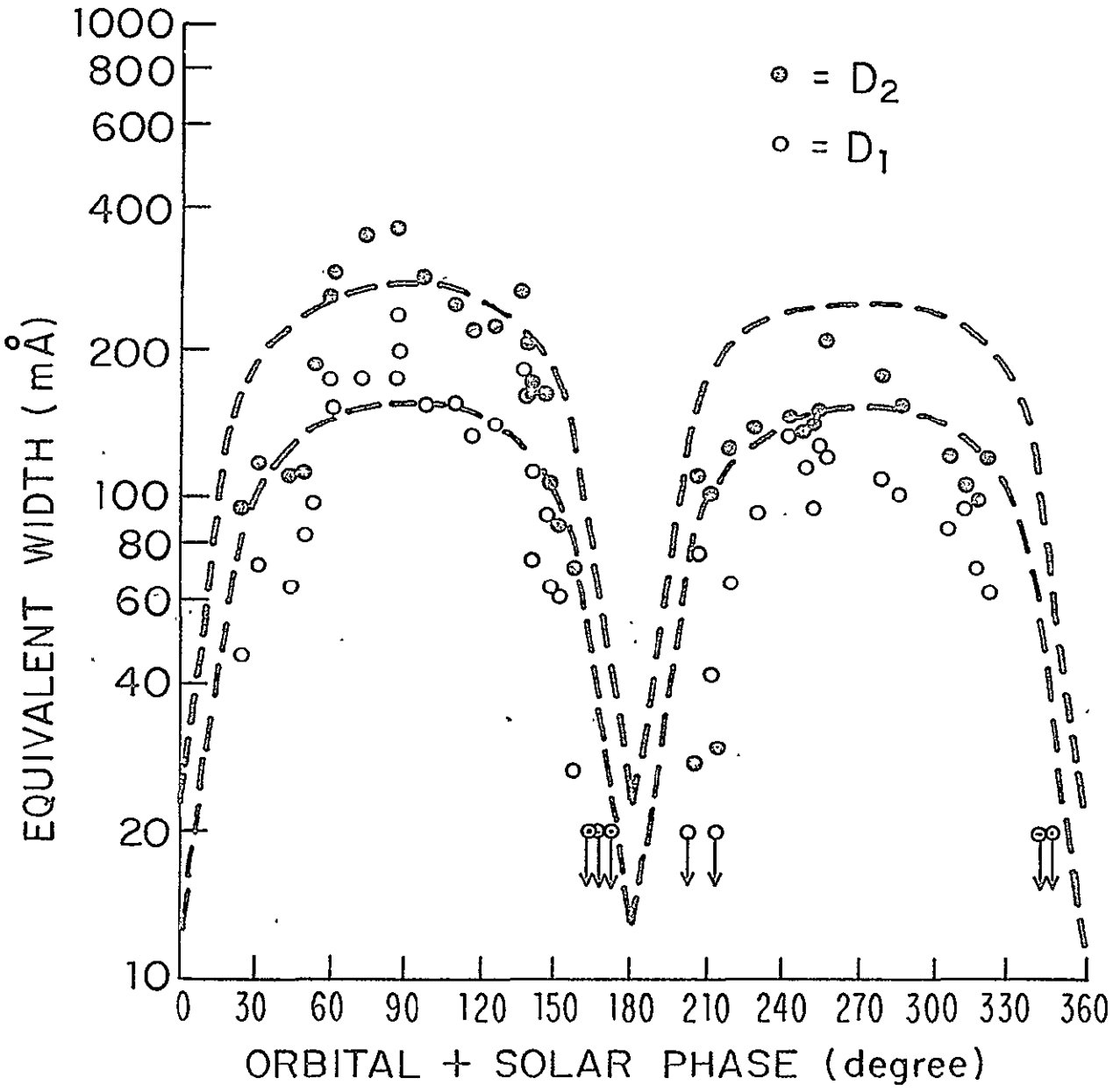

Figure 4. Bergstralh Intensity Asymmetry Data. The equivalent width to mean opposition continuum level of the sodium D-line emission measured by Bergstralh et al. (1975) is shown. The dashed curves are the solar excitation values for both D_2 and D_1.

ments show that the critical satellite phase angle for which the central axis of the forward cloud is approximately parallel to Earth-Jupiter line of sight is 65-75 degrees near eastern elongation and 230 degrees near western elongation. There is therefore an east-west phase lag asymmetry of about 15-25 degrees. This qualitative behavior was exhibited by the preliminary calculations shown in Figure 2 and discussed in Section 2.1 and resulted directly from the effect of solar radiation acceleration on the sodium cloud atoms. To obtain quantitative evaluation, detailed three-dimensional sodium cloud model calculations, modified to include the solar radiation acceleration, have been performed and are reported here.

Results for Io's three-dimensional sodium cloud model illustrating the perturbing effects of solar radiation pressure are given for satellite phase angles of 55 and 235 degrees in Figure 5 and Figure 6 respectively and may be compared directly with the simpler results of Figure 2. Model calculations assumed sodium was emitted radially from the inner hemisphere of Io's exosphere (2600 km radius) with a velocity of 2.6 km sec^{-1} and had a cutoff lifetime of 20 hours in the Jovian environment. The outer contour value is 916 Rayleighs for a surface flux of 10^8 atoms cm^{-2} sec^{-1}, with contours spaced by 367 Rayleighs, increasing inward toward Io. The results of Figure 5 and Figure 6 show that changes in the D_2 intensity pattern of the sodium cloud are not very sensitive to the illumination angle of the sun relative to the Earth-Jupiter line of sight. The sun angle is confined to values

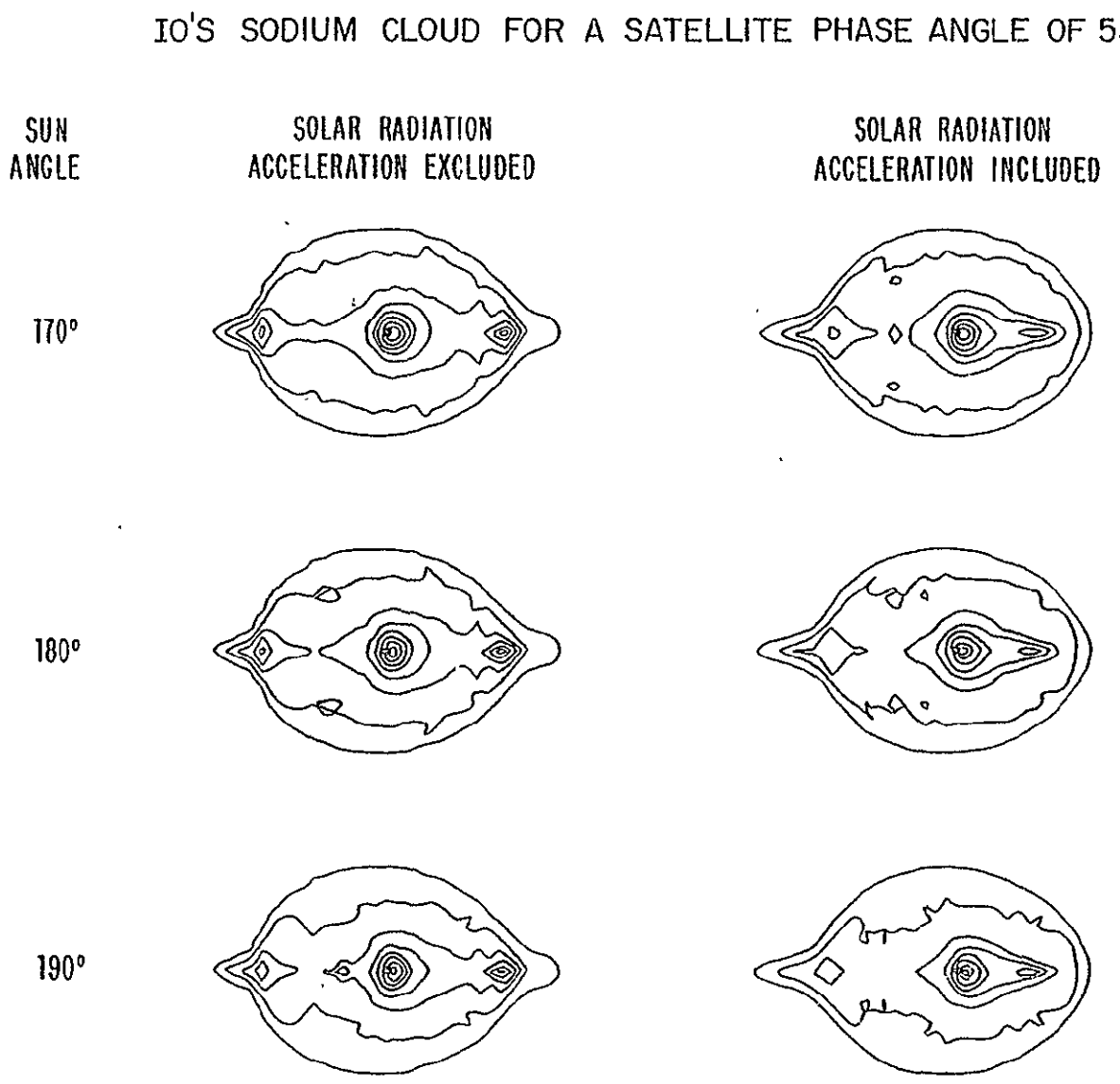

Figure 5. Effects of Solar Radiation Pressue in the East Cloud. Calculated D_2 intensity contours of the sodium cloud are compared, with and without the effects of solar radiation pressure, for the indicated phase and sun angles. See text for discussion.

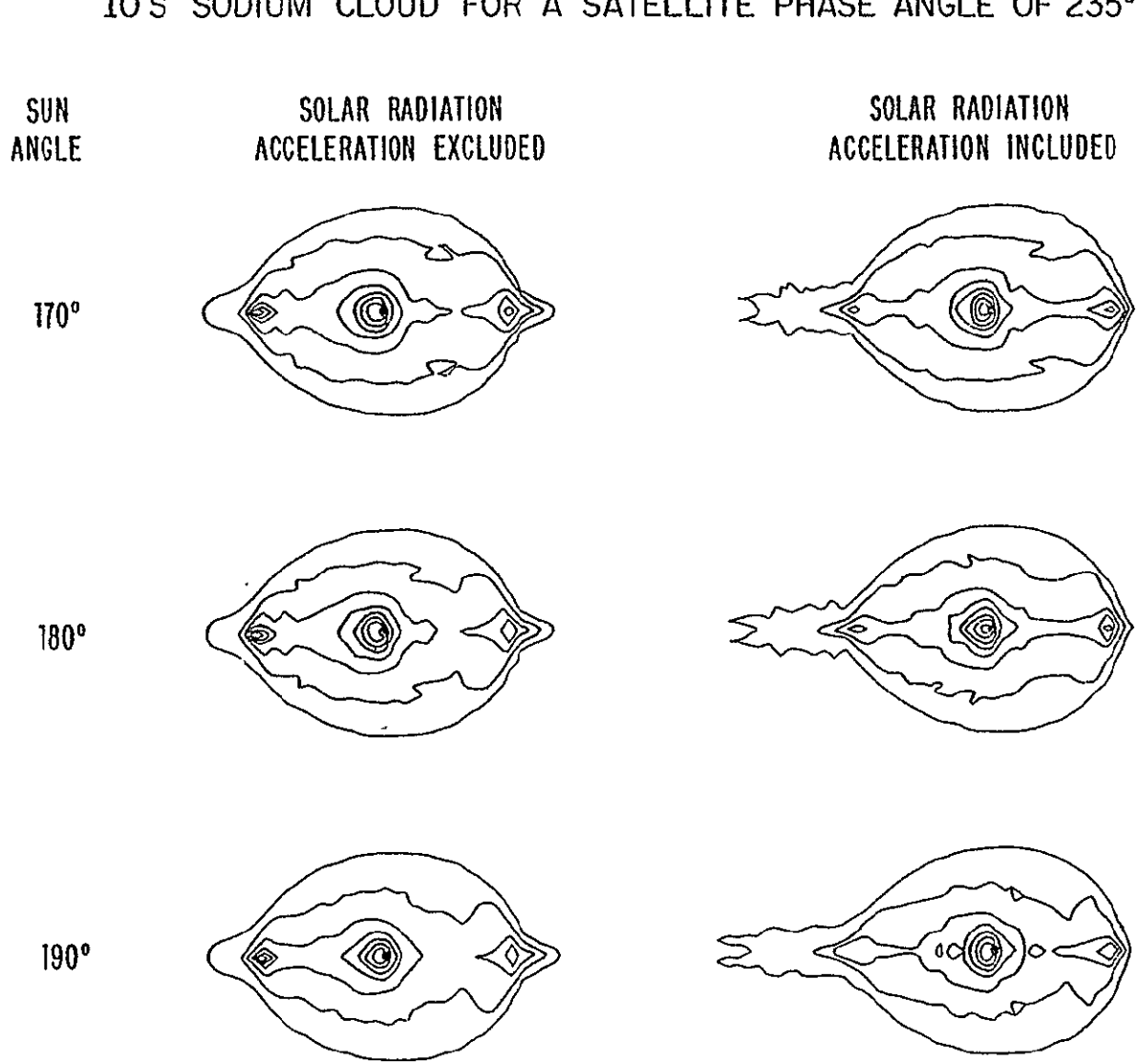

Figure 6. Effects of Solar Radiation Pressure in the West Cloud. Same description as Figure 5.

between about 167 and 193 degrees as the Earth moves about the Sun. For a sun angle of 180 degrees, the Earth-Jupiter line of sight and the Sun-Jupiter axis of Figure 2 are identical. For a satellite phase angle of 55 degrees, note that in Figure 5 the effect of solar radiation is to rotate the central axis of the forward elongation sodium cloud further away from Jupiter as anticipated in the results of Figure 2. The inner edge of the cloud (right portion) in Figure 5 is therefore closer to Io while the outer edge (left portion) is extended further from Io. For a phase angle of 235 degrees, note that in Figure 6 the solar radiation pressure has effectively rotated the sodium cloud axis more toward Jupiter as anticipated in Figure 2. The outer edge of the cloud (right portion) in Figure 6 is therefore closer to Io while the inner edge of the cloud (left portion) clearly reveals that the axis of the forward elongated sodium cloud has already begun to swing through our line of sight.

The model calculations of Figure 5 and Figure 6 confirm that solar radiation pressure introduces an east-west phase lag asymmetry into the spatial distribution of the sodium cloud. The central axis of the forward elongated cloud is not therefore aligned along the Earth-Jupiter line of sight for diametrically opposite satellite phase angles east and west of Jupiter. The observations of Goldberg and colleagues (1978) indicate that this east-west phase lag asymmetry is about 15 to perhaps 25 degrees. In the absence of solar radiation pressure, the D_2 intensity pattern of the sodium cloud

for diametrically opposite satellite phase angles is presented in Figure 7, where the sun angle is 180 degrees and the other model parameters and contour levels are the same as in Figure 5 and Figure 6. Note that the east and west intensity patterns are effectively mirror images of each other, and that the axis of the forward elongated cloud can be seen to swing through our line of sight at a phase angle of about 55 degrees in the east and 235 degrees in the west, yielding no phase lag. The observed changes in the intensity pattern of the cloud with satellite phase angle are almost completely due to the changing geometric viewing perspective of the cloud projected onto the plane of the sky.

The observations of Goldberg et al. (1978) and Goldberg (1979) indicate that the soidum cloud appears nearly symmetric about Io at an eastern elongation phase angle of 65 to perhaps 75 degrees and at a western satellite phase angle of 230 degrees. In Figure 8, results for the D_2 intensity pattern of the sodium cloud are shown and compared for diametrically opposite satellite phase angles east and west of Jupiter, where solar radiation pressure has been included in the model calculations. Near eastern elongation, note that the sodium appears symmetric near a satellite phase angle of about 65 degrees, whereas near western elongation the cloud appears symmetric at a phase angle of 230 degrees. This produces an east-west phase lag asymmetry of about 15 degrees and is in excellent agreement with observations. Note that in Figure 8, the passage of the forward cloud axis through our field of

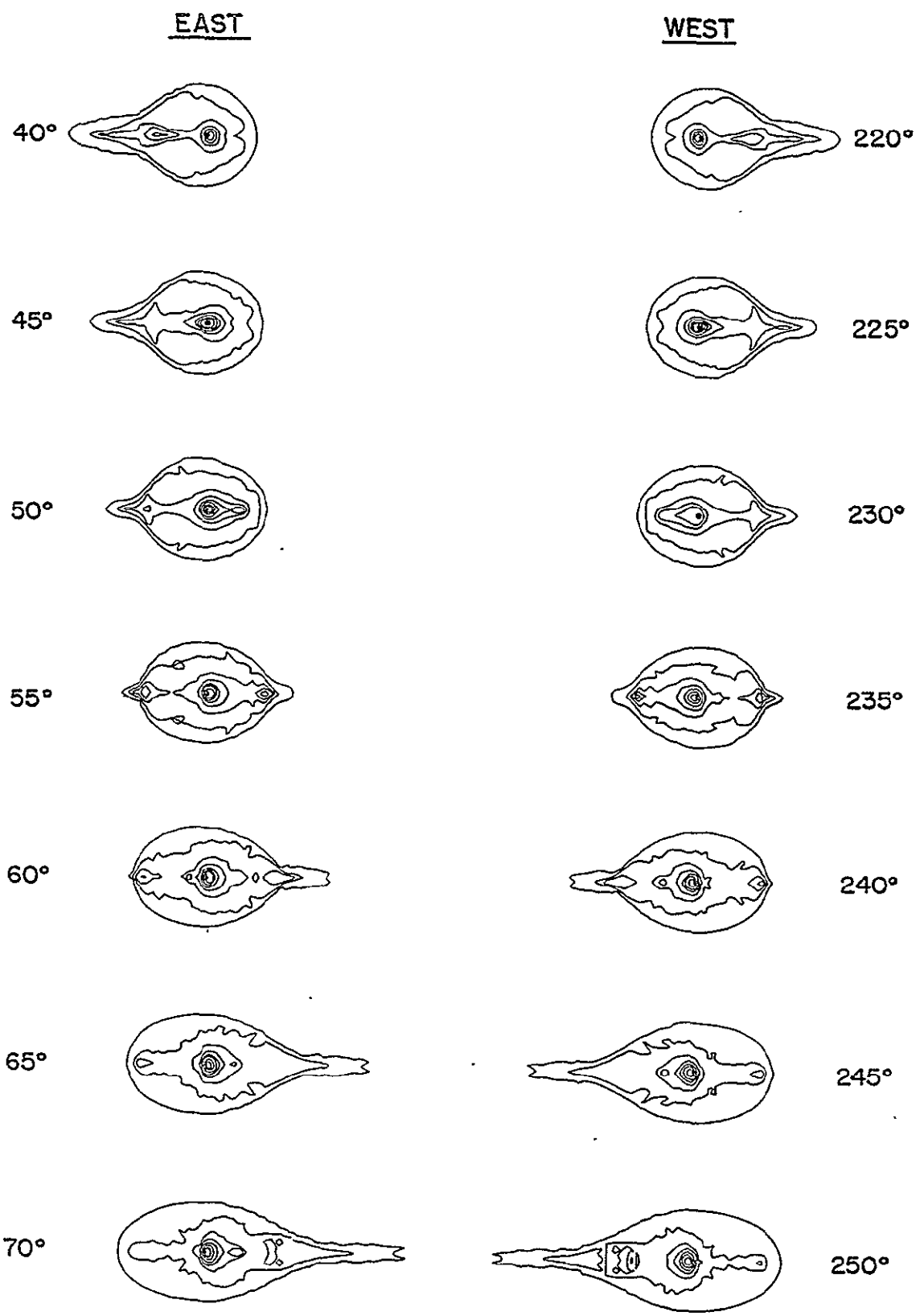

Figure 7. Goldberg Asymmetry Model Results.
Model calculations of the D_2 intensity contours, excluding the effects of solar radiation pressure, show no Goldberg phase lag asymmetry.

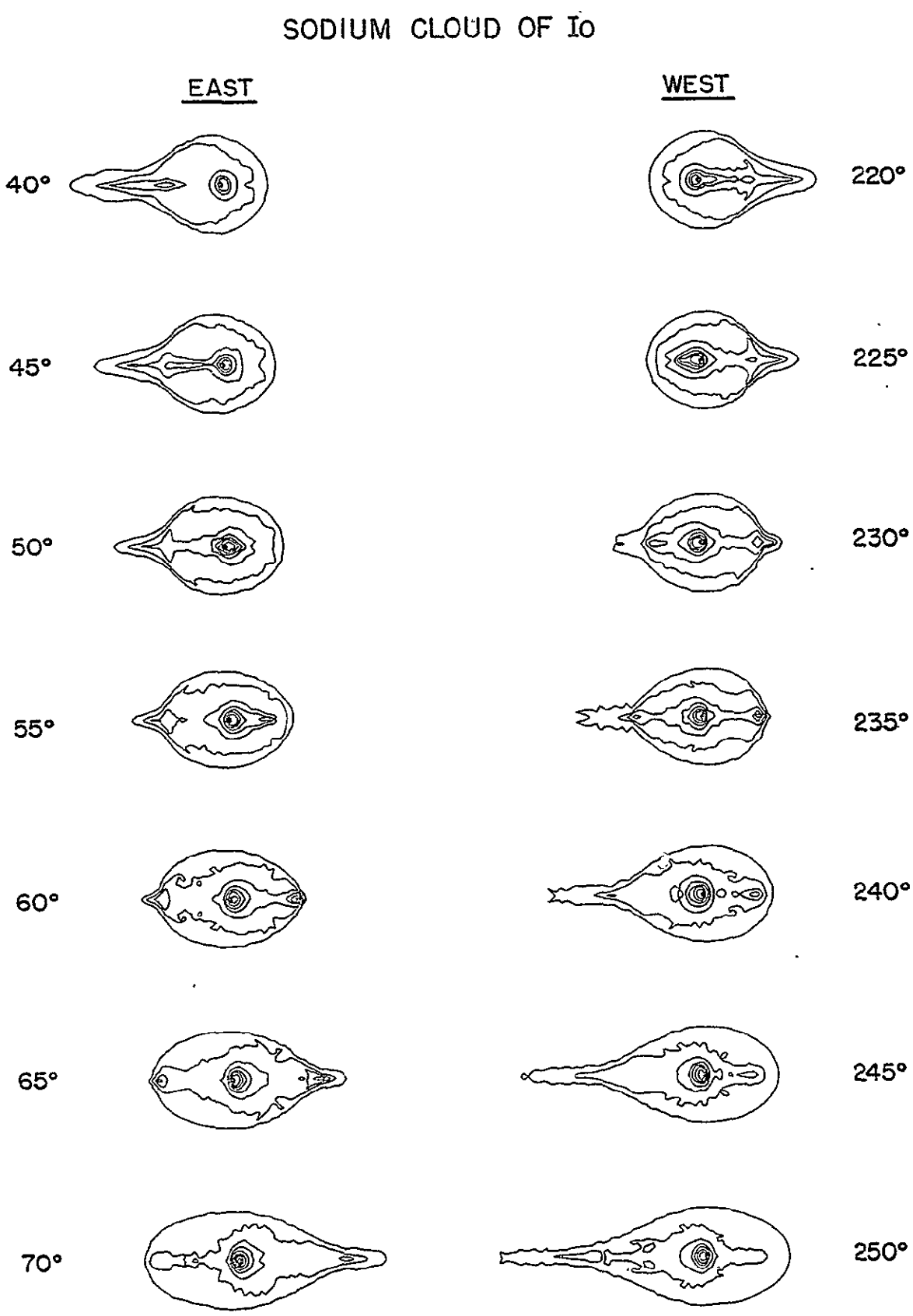

Figure 8. Goldberg Asymmetry Model Results.
Model calculations of the D_2 intensity contours of the sodium cloud, including the effects of solar radiation pressure, clearly show the Goldberg phase lag asymmetry.

view is much less definite in the east than in the west. This makes it more difficult to accurately determine the eastern critical satellite phase angle, a problem also encountered in the observational data of Goldberg (1979).

The results of Figure 7 and Figure 8 are calcualted assuming a monoenergetic emission velocity of 2.6 km sec^{-1}. Results for lower emission velocity components that would be included if a more realistic initial emission velocity distribution were adopted, are shown in Figure 9 and Figure 10 for diametrically opposite phase angles east and west of Jupiter. The D_2 intensity images, with the same contour levels chosen in Figure 5, indicate that the lower emission velocity components are very important in determining the overall intensity distribution of the sodium cloud near Io. The critical satellite phase angle for an emission velocity of 2.2 km sec^{-1} has increased to 70 degrees in the east and to slightly over 230 degrees in the west. This indicates that a phase lag of 15 to 20 degrees would also be present if an initial velocity distribution were adopted and that such a distribution can be expected to give excellent agreement with the observations.

2.3 Model Results: Bergstralh's Intensity Asymmetry

Detailed three-dimensional model calculations to test the ability of the solar radiation pressure mechanism to explain the east-west intensity asymmetry of Bergstralh et al. (1975, 1977) have been performed. Results have shown that the Bergstralh asymmetry depends critically upon the components of the

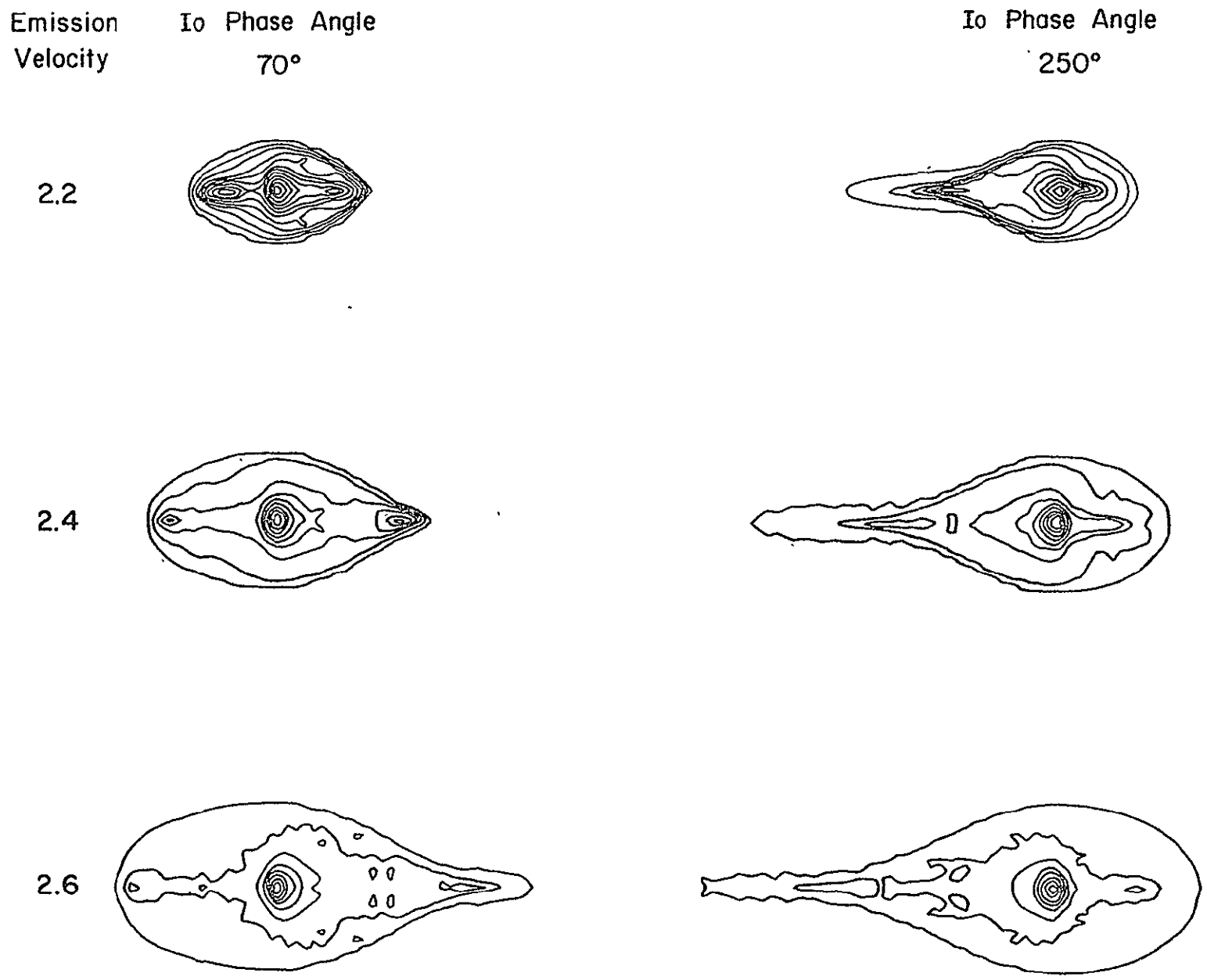

Figure 9. Emission Velocity Dependence. Calculated D_2 intensity contours of the sodium cloud, including solar radiation pressure effects, are compared as a function of emission velocity.

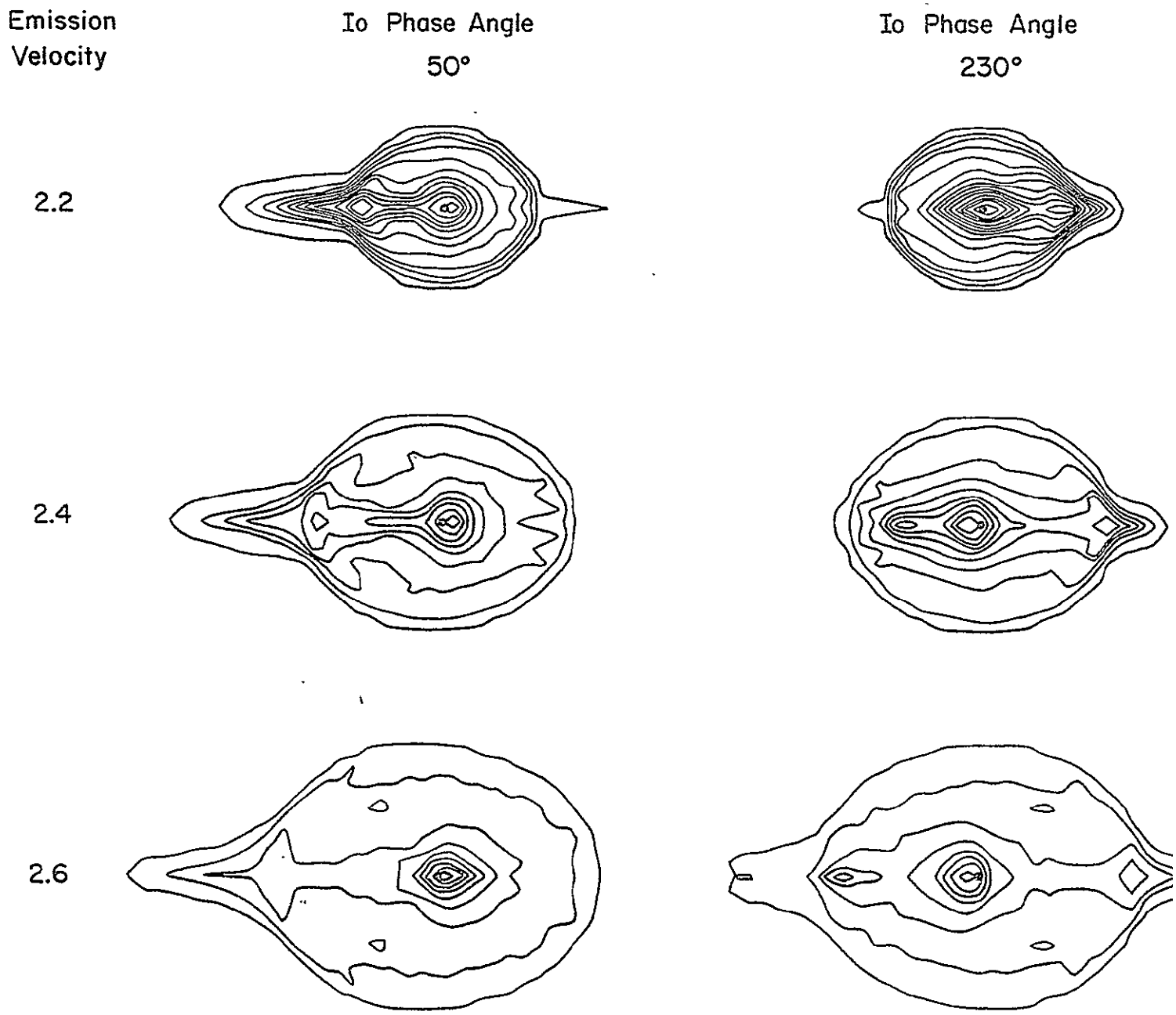

Figure 10. Emission Velocity Dependence.
Same description as Figure 9.

emission velocity dispersion of the sodium atom unlike the Goldberg asymmetry. In performing the calculations, the most interesting question arises as to how the D-line solar radiation acceleration, representing only a 1 to 2% perturbation in Jupiter's gravitational acceleration of a sodium atom at Io's orbit (see the Appendix), can make a 20 to 25% east-west change in the D_2 intensity of the cloud measured through the observing slit (see Figure 3) used by Bergstralh and colleagues. The answer is not immediately obvious.

To understand the impact of solar radiation pressure on the sodium intensity seen through the observation slit, centered on Io, it is of importance to realize that the lower velocity components of the initial atom emission velocity distribution contribute more significantly to the intensity than the higher components. This occurs because, for the lower components, the cloud is concentrated into a smaller volume and therefore provides a larger column density. There is, of course, a lower limit to the emission velocity for this effect, which occurs when the sodium atoms can no longer escape the gravitational field of Io and populate the cloud. This occurs for initial velocities less than about 1.8 km sec^{-1}. The question is then how can solar radiation pressure significantly modify the orbits of these more important lower velocity components. The answer is found in considering the forces acting on such a sodium atom.

The force $\vec{F}$ on a sodium atom in a coordinate frame rotating with Io is given by

$$\vec{F} = \vec{F}_I + \vec{F}_J + \vec{F}_\Omega + \vec{F}_R$$

where $\vec{F}_I$ and $\vec{F}_J$ are respectively the gravitational forces of Io and Jupiter, where $\vec{F}_\Omega$ is the centrifugal force introduced by the rotating frame, and where $\vec{F}_R$ is the solar radiation pressure force. For initial velocities larger than about 1.8 km sec^{-1}, sodium atoms have sufficient energy to penetrate the Lagrange sphere ($\sim$5.8 satellite radii from Io), the sphere on which the combined forces

$$\vec{F}_I + \vec{F}_J + \vec{F}_\Omega$$

nearly cancel. The near cancellation of forces actually occurs in a spatial volume, approximately given by a spherical shell about the Lagrange sphere. Inside the Lagrange shell, the relative contribution of $\vec{F}_R$ to $\vec{F}$ is greatly enhanced.

For sodium atoms which have sufficiently large initial velocities ($\gtrsim$2.2 km sec^{-1}) so that they move through the Lagrange shell more rapidly, there is not time for the force $\vec{F}$ to alter the atom trajectory significantly. However, for initial velocities below this value and slightly above the ballistic level, the penetration time is significantly long so that the atom orbit may be significantly altered by the force $\vec{F}_R$ in the Lagrange shell. The forces $\vec{F}_I$, $\vec{F}_J$ and $\vec{F}_\Omega$ do not depend upon the satellite phase angle. The force vector $\vec{F}_R$, however, is reversed in the rotating coordinate frame for satellite phase angles separated by 180 degrees. By this

mechanism the force $\vec{F}_R$ is able to introduce a significant east-west asymmetry in the atom orbits.

Model calculations of the relative D_2 intensity seen through the observation slit of Bergstralh et al. (1975, 1977), shown in Figure 3 and taken here to have nominal dimensions of 9×10^3 km by 2.4×10^4 km, are presented in Figure 11. The relative D_2 intensity is shown as a function of the satellite phase angle for four different emission velocities spanning the range from 2.0 km sec^{-1} to 2.6 km sec^{-1}. The intensity, calculated for atom emission from the inner hemisphere, includes the shadow effect of the disk of Io blocking the cloud behind it and assumes that the tilt angle of the satellite plane is zero relative to the observer and that the sun angle is 180 degrees.

The model calculations of Figure 11 clealry show that solar radiation pressure introduces a large east-west intensity asymmetry for the initial emission velocity of 2.0 km sec^{-1} and a somewhat less pronounced asymmetry for the 2.1 km sec^{-1} emission velocity. The asymmetry is not present for the higher emission velocities of 2.4 km sec^{-1} and 2.6 km sec^{-1}. Note that the contributions to the intensity have a maximum value at 50 to 60 degrees in the east and at 230 degrees in the west. The maximum intensity of the 2.0 km sec^{-1} results is 4.38 times larger than the 2.6 km sec^{-1} results in the east and 3.48 times larger in the west.

The east-west ratio of the relative D_2 intensity for the 2.0 km sec^{-1} and 2.1 km sec^{-1} emission velocities is presented

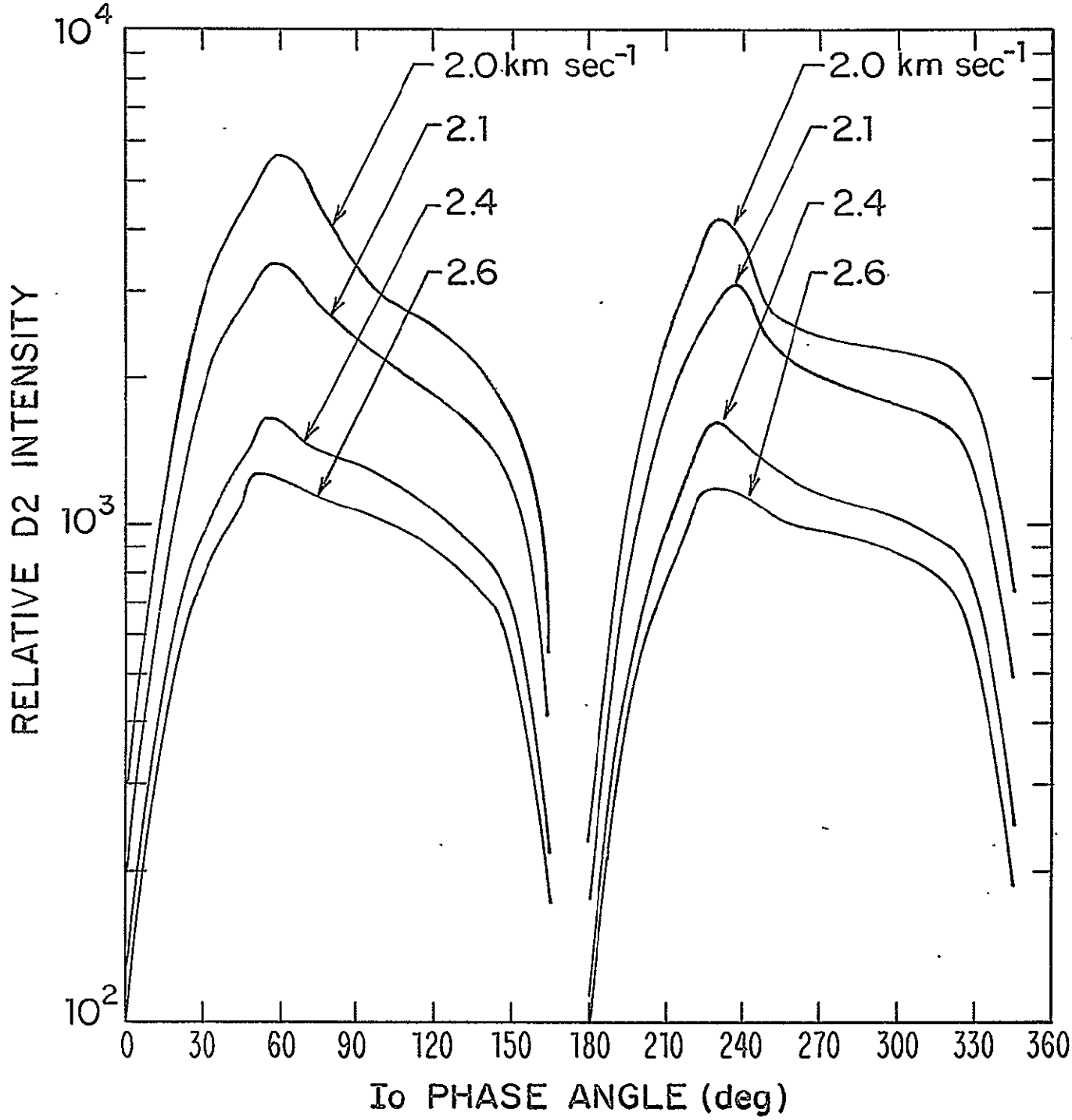

Figure 11. Model Results for the Bergstralh Intensity Asymmetry. The calculated relative D_2 intensity of the sodium cloud seen through the rectangular slit of Bergstralh et al. (1975, 1977) is shown as a function of Io phase angle for different emission velocities. See text for discussion.

in Figure 12, where the results of including and excluding the effects of Io's shadow are both indicated. Note that the ratio for the 2.0 km sec^{-1} velocity provides a minimum east-west asymmetry of 17 percent over most of the angular range when the shadow is included, and at a 70 degree phase angle has a peak value in excess of 80 percent. The 2.1 km sec^{-1} ratio is less pronounced, but still provides a significant east-west asymmetry over much of the phase angle interval. The maximum observed signal reported by Bergstralh et al. (1977) using their best data base was 241 k Rayleighs occurring at a satellite phase angle near eastern elongation and assumed to uniformly illuminate a 3 x 3 arc second portion of the observation slit. For a 3 x 8 arc second slit this uniform intensity is reduced to about 90 k Rayleighs. If this intensity were produced by the maximum D_2 intensity given by the 2.0 km/sec calculation of Figure 11, a satellite flux of order $1x10^8$ atoms cm^{-2} sec^{-1} would be required, in agreement with an earlier estimate by Smyth and McElroy (1978).

The results of Figure 11 and Figure 12 would suggest that the velocities near 2.0 km sec^{-1} play a major role in the actual initial velocity distribution of sodium atoms in the Io atmosphere. For velocity components of 1.9 km sec^{-1} and lower, ballistic orbits begin to dominate and the cloud becomes less bright and is mostly confined inside the Lagrange sphere where the asymmetric mechanism is not operative. Inversion of the sodium data of Bergstralh et al. (1975, 1977) to obtain the initial emission velocity distribution is clearly

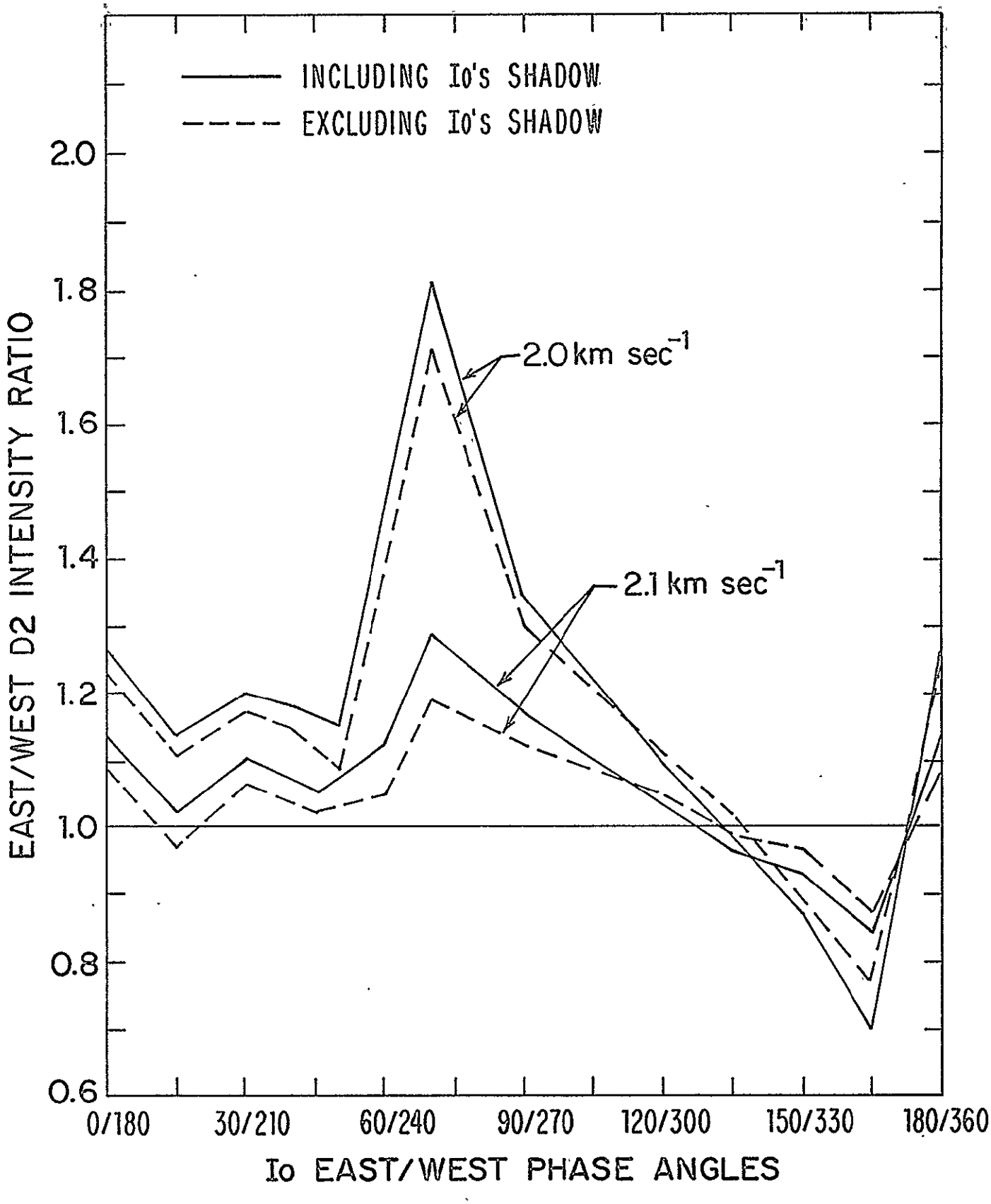

Figure 12. Bergstralh East-West Intensity Ratio. The east/west D_2 intensity ratio of Figure 11 is shown as a function of the east/west phase angles for a 2.0 km/sec and 2.1 km/sec emission velocity.

a desirable modeling goal. Modeling results such as those in Figure 11 are critical in such an inversion process. However, the results of Figure 11 need to be recalculated so as to include the non-uniform spatial lifetime of sodium atoms produced by the presence of the Io plasma torus. With these new results such an inversion process would be meaningful. The results of Figure 11, calculated assuming a 20 hour cut-off lifetime model for sodium, may be modified significantly by the plasma torus, since the lifetime of sodium atoms near Io's orbit would then be reduced to a value of order one hour. The effect of the plasma torus on the sodium cloud is discussed more fully in Chapter III. This additional refinement in modeling is clearly warranted to properly understand the sodium cloud escape mechanism. It should also serve as a basis of understanding the more general escape problem of sulfur and oxygen from Io and the manner in which ions and energy are supplied to the plasma torus.

CHAPTER III

IO'S SODIUM CLOUD: LINE PROFILES

3.1 Introduction

The sodium cloud of Io may be investigated by studying the shape of the line profiles of the D_1 and D_2 wavelength emission. Such a study is complementary to the two-dimensional modeling analysis of Chapter II and should provide a direct and more sensitive method of determining the initial velocity dispersion of atoms emitted by the satellite.

Discovery of Io's sodium cloud in 1973 by Brown (Brown, 1974; Brown and Chaffee, 1974) came about by observation of the D-line emission profiles. Later higher-resolution observations (Trafton, 1975; Trauger et al., 1976; Trafton and Macy, 1977) have revealed in detail the velocity dispersion of the sodium atoms in the larger cloud. Models for the line profile data (Smyth and McElroy, 1977; Trafton and Macy, 1978; Carlson et al., 1978; Macy and Trafton, 1980) have generally drawn similar conclusions. Much modeling work, however, remains in order to better understand the velocity structure in the line profiles and to determine the initial velocity distribution of sodium atoms emitted by Io. The understanding and interpretation of these line profile features are current goals of our modeling program. Preliminary results, indicating recent progress, are reported.

3.2 Review of Observational Data

A brief summary of the relevant characteristics of the sodium line profiles and their physical implications is in order to provide necessary background information for modeling. The line profiles have two striking characteristics first observed by Trafton (1975) and further clarified by Trafton and Macy (1977). The first feature is a tall emission peak, shifted 0-50 ma from the Io rest frame and having a variable half-width of about 30-70 ma. The peak of the emission is shifted to wavelengths which are longer than the wavelength of the D-lines in Io's reference frame when Io is west of Jupiter and it is shifted to shorter wavelengths when Io is east of Jupiter. The magnitude of the shift appears to be correlated with Io's orbital phase angle (Trafton and Macy, 1977). This shift and phase angle dependences of the peak are also confirmed by sodium data of Trauger et al. (1976).

The second and more obvious feature of the sodium line profile is the presence of an extension or skirt asymmetrically attached to one side of the emission peak. The asymmetry is very pronounced and is more prominent on the short-wavelength side of the peak when Io is east of Jupiter, while being more prominent on the long-wavelength side of the peak when Io is on the west side of Jupiter. The skirt is largest when Io is on Jupiter's magnetic equator (Trafton and Macy, 1977) with a skirt base-width varying from about 120 to nearly 500 ma, measured relative to the peak. This skirt asymmetry has also been observed by Trauger et al. (1976) and Carlson et al.

(1978) and does not depend upon having Io in the viewing aperture of the instrument.

Interpretation of the sodium line profile data has proceeded with the aid of sodium cloud models based on trajectory calculations. An explanation for the asymmetric skirt was suggested first by model calculation of Smyth and McElroy (1977). Their modeling showed that emission of sodium by the inner-leading guadrant of the satellite with a mean velocity of about 3 km sec^{-1} and a dispersion in emission velocities with speeds ranging up to about 15 km sec^{-1} would provide both the correct shift of the peak and the proper asymmetry to the skirt. Initial modeling by Trafton and Macy (1978) favored emission of sodium in the forward direction of Io's motion (leading hemisphere or expansion parallel to Io's orbital velocity), while their later more extensive analysis (Macy and Trafton, 1980) preferred high veloicty emission of sodium from the leading-inner quadrant (with speeds up to 13 km/sec) to explain the skirt asymmetry. Modeling of Carlson et al. (1978) preferred emission of sodium from the leading hemisphere of the satellite with a veloicty distribution centered at about 2.5 km sec^{-1} and a dispersion, similar to the sputtering velocity distribution they adopted, characterized by a long velocity tail with speeds up to 15 km sec^{-1}. With this preliminary modeling consistency among investigators, future analysis may be broadened to seek consistent modeling for both the line profile data and the two-dimensional data. The constraint of these two data sets provides an excellent

means of refining our knowledge of the initial velocity dispersion and the surface flux distribution of sodium emitted by Io. Preliminary results are presented in the next section.

3.3 Preliminary Modeling Results

In Chapter II interest was focused upon understanding the spatial distribution of the sodium cloud near Io and its associated east-west asymmetries as a function of phase angle. Interest will now be directed to understanding the characteristics of the line profiles produced by the sodium cloud of Chapter II and comparing them to the observed line profile data reviewed in Section 3.2. Line profile calculations presented will therefore assume the same model parameters adopted in Chapter II - that sodium is emitted continuously, uniformly and radially from the inner hemisphere of Io's exosphere (2600 km in radius) having an initially specified speed, and a lifetime of 20 hours in the Jovian environment. The effect of solar radiation pressure on the line profiles is also included. Line profiles presented are calculated for the D_2 radiation intensity seen through a circular aperture of radius 2.6×10^4 km (about 7-9 arc sec) centered on Io. Line profiles produced by low emission velocities (1.8 to 2.2 km sec^{-1}) are characterized by tall, narrow peaks incapable of explaining either the peak shift or the skirt asymmetry seen in the data. A velocity of 2.6 km sec^{-1}, adequate for our present purposes, has therefore been adopted for the preliminary modeling results.

Model line profiles are presented in Figure 13 for each of the cloud images shown in Figure 8, which assumed an emission velocity of 2.6 km sec^{-1}. The size of the adopted circular line-profile aperture is indicated in Figure 14 for the cloud image having a 55 degree satellite phase angle. The line profiles are basically composed of two different parts: (1) a large central peak arising from the velocity dispersion in the near dense Io cloud, and (2) a lower and generally much wider asymmetric contribution produced by the forward portion of the Io sodium cloud.

The central peaks of the line profiles shown in Figure 13 are shifted by about 30 ma from the Io rest frame wavelength and reflect the fact that atoms initially emitted from the inner hemisphere at 2.6 km sec^{-1} have, upon escaping Io, a velocity in the forward cloud directed with a speed centered at 1.5 km sec^{-1}. The peak is therefore shifted to shorter (negative) wavelengths than the D_2-line emission in Io's reference frame when Io is east of Jupiter and it is shifted to longer (positive) wavelengths when Io is west of Jupiter. The width and shift of the peak are thus basically determined by the initial emission velocity magntiude chosen in the calculation and the changing orientation of the inner hemisphere along the observer's line of sight with satellite phase angle. This sign and magnitude of the calculated peak shift are the same as observed for the peak shifts of the line profile data discussed in Section 3.2. Solar radiation pressure causes slightly larger central peak shifts for western satellite

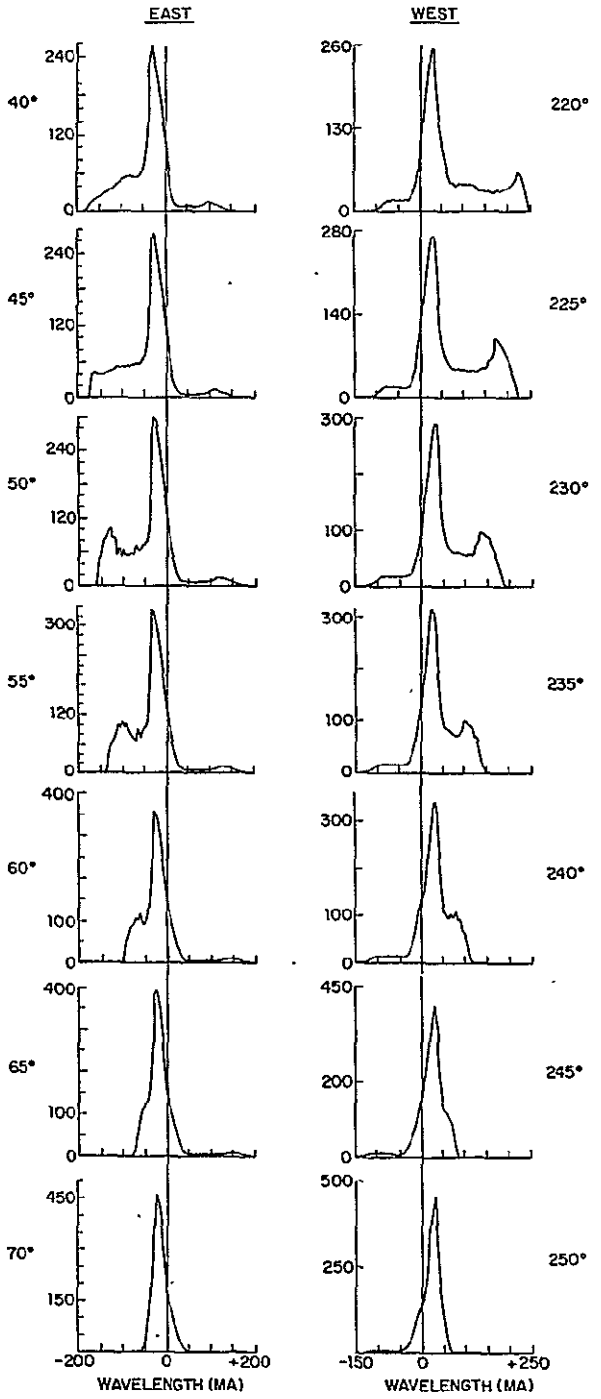

Figure 13. Model Results for Sodium Line Profiles. The calculated D_2-line profile shapes seen through the circular aperture shown in Figure 14 are compared for diametrically opposite phase angles east and west of Jupiter. See text for discussion.

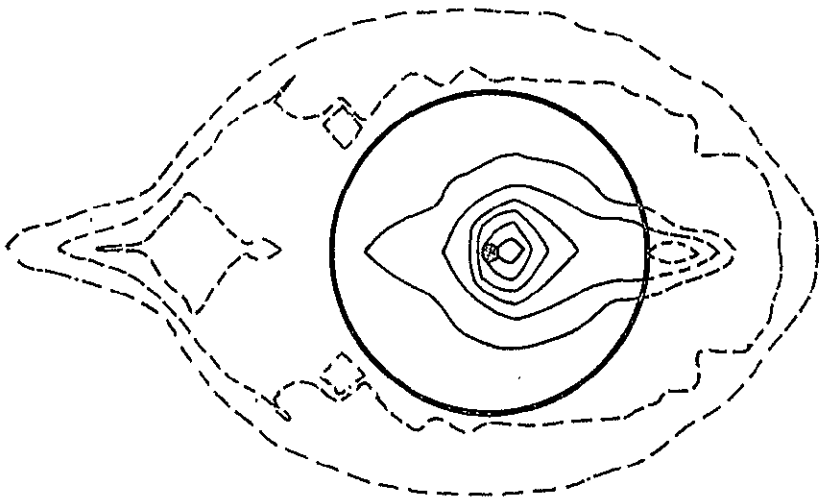

Figure 14. Line Profile Aperture. The relative size of the aperture used in the calculated line profiles of Figure 13 is shown in relationship to the sodium cloud model results of Figure 8 having a phase angle of 55 degrees.

phase angles than for eastern ones. For the phase angles of 40 and 220 degrees, the shifts are respectively about -30 ma and +34 ma. Larger values of the emission velocity will give larger shifts.

The asymmetric skirt connected to the central peak in Figure 13 is produced by the forward portion of the sodium cloud evident in the images of Figure 8. For eastern phase angles between 40 and 65 degrees, the forward cloud contribution is clearly seen and occurs for wavelengths shorter than the D_2-line wavelength in Io's reference frame. The base width of the skirt for a phase angle of 40 degrees is about -165 ma, measured relative to the central peak. The skirt can be seen for western phase angles between 220 and 245 degrees and occurs for wavelengths longer than the D_2-line wavelength in Io's rest frame. This positioning of the skirt relative to the central peak for eastern and western phase angles is in the same sense as the asymmetric skirt seen in the sodium line profile data. Higher velocities in the forward cloud near western elongation, produced by solar radiation pressure, provide an increased western skirt width. At a 220 degree phase angle for example, the skirt width relative to the central peak is about 210 ma, in contrast to the -165 ma value for a 40° phase angle. Superposition of many such monoenergetic calculations to produce an initial emission velocity distribution for the satellite will therefore tend to produce a line profile having a smaller full width at half maximum at eastern elongation than at western elongation.

Such an east-west trend can, in fact, be seen in the line profile data of Trafton (1975) and Trafton and Macy (1977).

In the east as the phase angle increases from 40 to 45 to 50 degrees, more of the forward cloud can be seen through the circular aperture (see Figure 14 and Figure 8) and this produces a second peak in the line profile. Similar behavior is seen for western phase angles except the event happens earlier because of the Goldberg phase lag asymmetry. As the eastern phase angle is increased beyond 60 degrees, the second peak in Figure 13 begins to merge with the central peak of the line profile. For phase angles in excess of 70 degrees in the east and 250 degrees in the west, the forward cloud has essentially passed through the circular viewing aperture and can no longer be seen. Thus only the central peak remains, arising from the low velocity portion of the sodium cloud near Io that is still in the field of view.

Line profile data (Trafton, 1975; Trafton and Macy, 1977; Trauger et al., 1976) for phase angles in excess of 70 degrees in the east and 250 degrees in the west show asymmetric skirts, in contrast to our modeling results. This suggests that additional higher-velocity components to complete an initial velocity distribution for the atoms emitted by the satellite are needed in the model to match the observed sodium line profile data. The velocity vectors of such sodium atoms would have to be approximately tangential to the satellite orbit at Io's location in order to be seen in the circular aperture for satellite phase angles in the range 70 to 120

degrees in the east and 250-300 degrees in the west. The magnitude of the velocity vectors would need to range up to perhaps 15 or 20 km sec^{-1} to produce the skirt width observed.

This set of circumstances suggests the possibility that high speed sodium atoms may be produced by the Jupter magnetospheric wind which moves past Io with a speed of about 56 km sec^{-1}. This idea is reinforced by the fact that the width of the line profile skirt is largest when Io is on Jupiter's magnetic equator. Such high speed sodium atoms assumed to be emitted from Io's leading hemisphere (Trafton and Macy, 1978; Carlson et al., 1978) or from Io's inner hemisphere (Macy and Trafton, 1980) have been included in previous modeling analyses. The addition of the high velocity sodium atoms component to our already established low velocity component shown in Figure 13 would provide a stronger skirt at low phase angles (40 to 70° in the east and 220 to 250 in the west) than at higher phase angels (70 to 120° in the east and 250-300° in the west). Cooperative efforts with ground based observational programs to provide new line profile data to clarify these points are in progress.

CHAPTER IV

IO'S SODIUM CLOUD: INTERACTION WITH IO'S PLASMA TORUS

4.1 Introduction

The presence of a high temperature plasma torus ($\sim 10^{5}$° K) approximately centered on the magnetic equatorial plane with the orbital radius of Io was recently discovered by the Voyager 1 spacecraft experiments (Broadfood et al., 1979; Bridge et al., 1979; Warwick et al., 1979) during its encounter with Jupiter. The vertical extent of the torus is approximately ±1 R_J (Jupiter radii) with an inner radius at about 5.3 R_J and an outer radius in excess of 7 R_J (Bagenal et al., 1980). Ion species detected in the torus include O^+, O^{++}, S^+, S^{++}, S^{+++}, S^{++++} and Na^+ as well as perhaps SO_2^+ or S_2^+, with electron number densities of order 2000 cm^{-3}. A lower temperature plasma torus ($\sim 10^{4}$° K) was discovered earlier by Kupo et al. (1976) through ground based measurements of excited state emissions from S^+ ions. The lower temperature plasma is located primarily inside Io's orbit, centered at about 5 R_J and with a vertical thickness of about ±1 R_J (Brown, 1978; Trauger et al., 1980; Pilcher and Morgan, 1980). The inner radius is located at about 4 R_J while the outer radius has been observed to be as large as 7 R_J (Pilcher and Morgan, 1980).

The high temperature plasma torus provides a strong sink for sodium atoms emitted by Io through electron impact ionization. The hot torus with an electron number density

of order 2000 cm^{-3} and a temperature of about 10^{5}° K (8.6 ev) can easily ionize sodium, with an ionization potential of 5.14 ev, in a time of about 1.8 hours. This small lifetime for sodium atoms in the hot plasma torus is in marked contrast to lifetime estimates of 20 hours (Smyth and McElroy, 1978) and 28 hours (Carlson et al., 1978) used in earlier modeling efforts. The lower-temperature plasma torus electrons, being less energetic, provide a longer lifetime, estimated to be about 8 hours by Brown (1976) for a characteristic density of $3.2x10^{3}$ cm^{-3} and a temperature of $2.5x10^{4}$° K.

The small sodium lifetime in the hot plasma torus of order one hour, upon first glance, might suggest that the sodium cloud would not be present during the Voyager 1 encounter. Earth-based measuremtns of Io's sodium cloud made during encounter by Goldberg et al. (1980), however, observed the overall shape and intensity of the sodium cloud essentially unchanged when compared to cloud measurements made at the same satellite phase angle in 1977. The sodium cloud near Io has in fact shown remarkable stability in intensity and shape over the last five years (Bergstralh et al., 1975, 1977; Matson et al., 1978; Murcray and Goody, 1978; Goldberg et al., 1980).

Within this stability a time modulation of the sodium cloud intensity has however been observed. This oscillating asymmetry in the intensity of the sodium cloud north and south of the satellite, correlated with Io's magnetic latitude, was discovered by Trafton and Macy (1975) and further

documented by Trafton (1977). This correlation was consistent with the interpretation that charged particles exist in greater concentration near the magnetic equator and remove sodium atoms from the cloud as it oscillates north and south of Io. This data, measured in 1974 and 1975, could be considered to be the first real detection of the Io plasma torus. The observed D-line emission intensity near the satellite when Io was on the magnetic equator was still quite evident (Trafton, 1977), indicating that the ionization rate of the plasma torus was not severe enough to eliminate the sodium cloud. Other short time variations in sodium cloud have recently been seen by Pilcher (1980) who observed bright linear features with irregular lifetimes. These linear features might be produced by either an enhanced sodium plumb source or by time-varying non-uniformities in the magnetosphere within the plasma torus.

Other longer time variations in the plasma torus properties are suggested by comparison of extreme ultraviolet observations of the torus by Voyager 1 and Voyager 2 (Sandel et al., 1979). These observations indicate changes by about a factor of 2 in the density and temperature of the plasma over a four month period. Such variations in plasma conditions could produce significant changes in the lifetime of sodium atoms and hence the cloud brightness. Even more pronounced changes in the hot plasma torus properties over a 6 year period are suggested by comparison of the absence of a 685 $\mathring{A}$ excited S^{++} emission in the UV photometer aboard

Pioneer 10 and the presence of a strong 685 Å signal in the UV spectrometer of Voyager 1 (Broadfoot et al., 1979).

4.2 Preliminary Modeling Results

Preliminary modeling results reported have been restricted to an initial investigation of the impact of the hot plasma torus upon Io's sodium cloud. The three-dimensional cloud model has been modified to include a spatial dependent lifetime for sodium atoms in the torus. This lifetime profile is determined by the spatial dependence of both the electron density and energy distribution.

The spatial variations of electron density within the hot torus are reasonably well known for the spacecraft inbound crossing of Io's orbit (Bagenal et al., 1980; Bridges et al., 1979). The energy distribution has not completely been reduced. It is however non-Maxwellian, having a cold component peaked at an energy of a few electron volts and a hot component of order 100 ev (Scudder, 1980). In the absence of this data reduction, the electron temperature is assumed, to first order, to be equal to the ion temperature, a spatial profile of which is given by Bagenal et al. (1980). The one-dimensional (radial) sodium lifetime profile, derived in this manner, is given in Figure 15, where a 20 hour background lifetime is assumed outside of the torus. Preliminary results presented here will use this first order lifetime profile. Two-dimensional (radial and vertical) lifetime profiles are under investigation. More accurate spatial information will

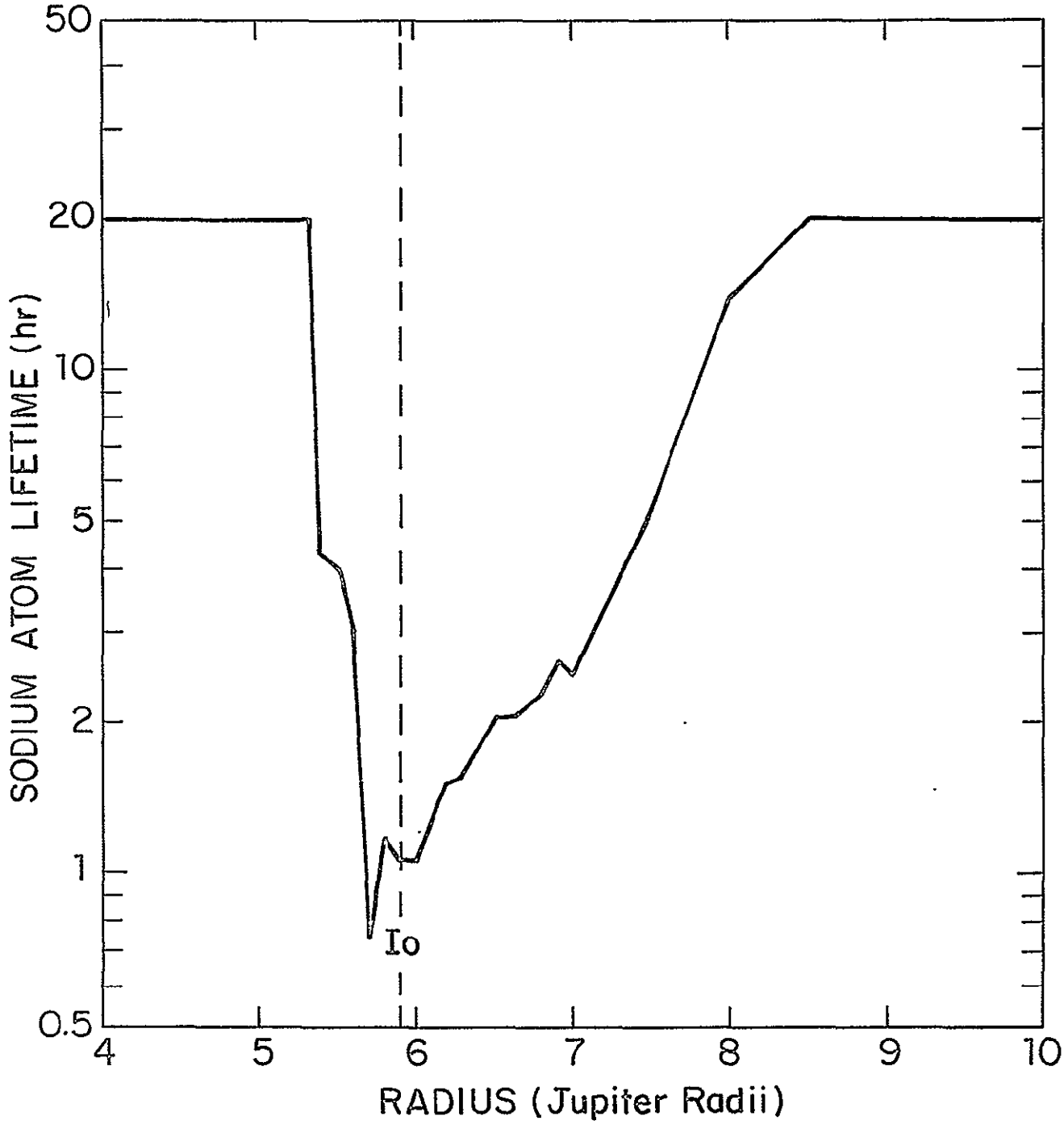

Figure 15. Sodium Lifetime Profile. The radial lifetime profile of sodium cloud atoms in the hot Io plasma torus along the centrifugal equilibrium equator is shown. See the text for discussion.

be incorporated in future lifetime calculations as it becomes available.

The sodium lifetime profile of the hot torus in Figure 15 is confined by the adopted 20 hour background to radial values between about 5.3 and 8.5 Jupiter radii. The profile is asymmetric about Io, increasing more rapidly as a sodium atom moves radially from the satellite orbit toward Jupiter than away from Jupiter. Because of this asymmetry, sodium atoms populating the forward portions of the cloud, which lies within Io's orbit, will have a greater probability of escaping the plasma torus before ionization than those atoms escaping from Io through the outer torus boundary. Previous models of the sodium cloud (Smyth and McElroy, 1978; Matson et al., 1978) indicate that sodium is emitted primarily from the inner hemisphere of the satellite. The question arises as to if the proposed hemispherical source is in effect an isotropic source with an asymmetric lifetime sink similar in nature to the profile of Figure 15.

Only a fraction of the sodium atoms emitted from Io will escape unionized from the hot plasma torus. In order for these escaping atoms to produce the correct brightness in the forward cloud, the actual satellite emission flux of sodium assumed in the model must be significantly increased beyond the value of 1×10^{8} cm^{-2} sec^{-1} (Smyth and McElroy, 1978), deduced from modeling efforts excluding the plasma torus lifetime effects. Such an enhancement of the flux will however introduce a significant intensity gradient

between the far forward cloud and the near Io portion of the cloud. This occurs since the sodium atoms closer to Io, having been emitted much more recently, have as yet not suffered as much ionization. The magnitude of this gradient however is limited by observations. The data of Bergstralh et al. (1975, 1977) provide an upper limit to the intensity very near Io (see Figure 3 and Figure 4) and cannot be exceeded. The data of Murcray and Goody (1978) and Matson et al. (1978) provide measurements of the sodium intensity in the far forward cloud. There is therefore an observational upper limit to the sodium emission flux enhancement that may be assumed in the model calculations.

Efforts to consistently model the interaction of the sodium cloud and plasma torus are currently in progress. Definite conclusions must await further analysis. Very preliminary results, indicating the progress of the research, are however reported. Observations by Murcray (1978) of the D_2 intensity of the sodium cloud at a satellite phase angle of 129 degrees are compared in Figure 16 with two model calculations which include the simple one-dimensional sodium plasma torus lifetime model of Figure 15. Both model results assume a monoenergetic emission velocity of 2.6 km sec^{-1} and were calculated for the observed satellite plane tilt angle of 3.265 degrees and the Sun angle of 178.6 degrees. A reasonable match of the intensity and location of the D_2 intensity contours in the forward sodium cloud is obtained if the model emission flux is assumed to be 5×10^9 cm^{-2} sec^{-1}.

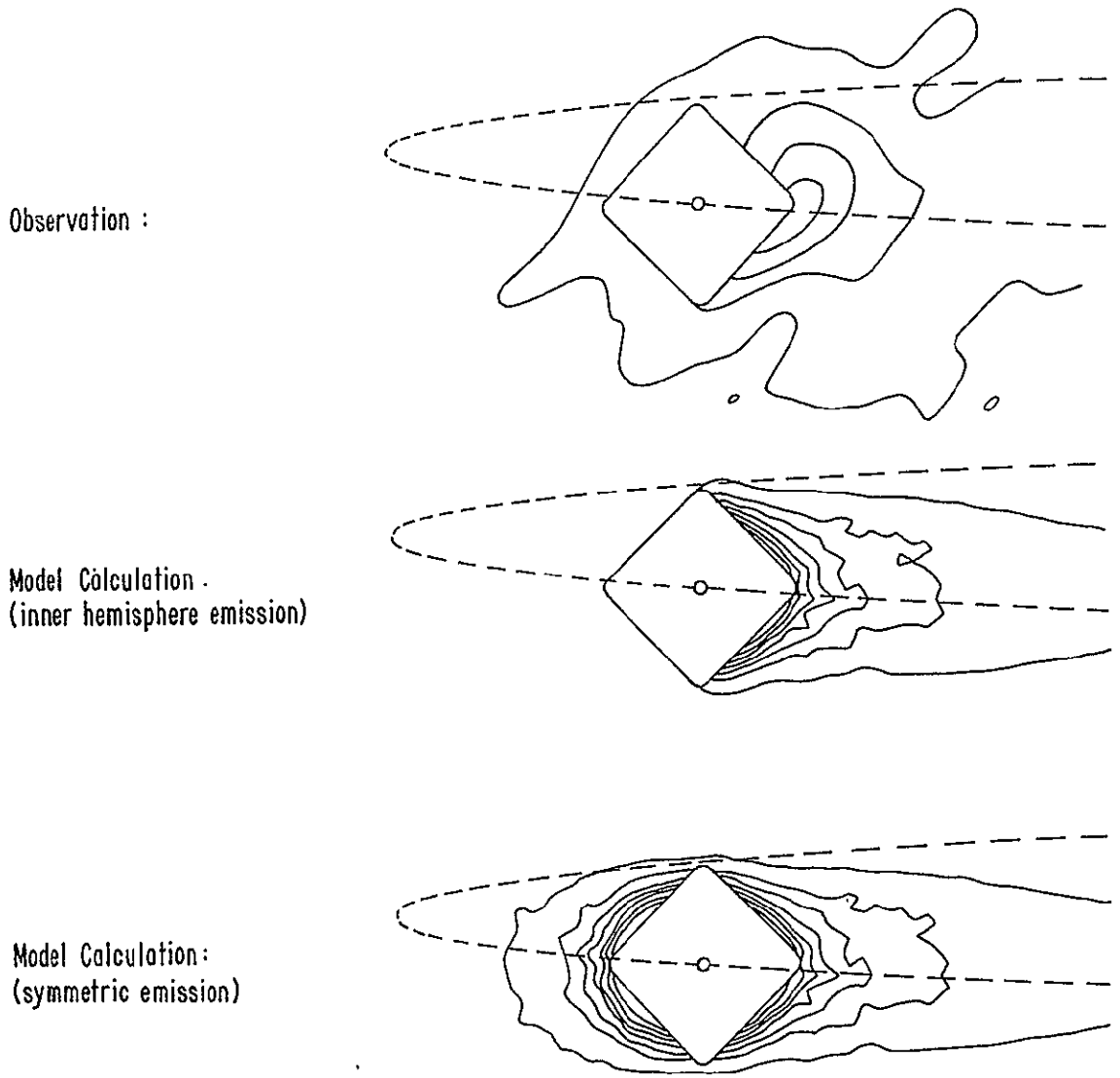

Figure 16. Plasma Torus Lifetime Model Results. The observed sodium cloud is compared with two model calculations, where the plasma torus sodium lifetime profile of Figure 15 is adopted. The outer D_2 intensity contours are 0.5 kR and inner contours increase by 1 kR steps. See text for discussion.

The vertical extent of the observed cloud is underestimated by the model since the increase of the sodium lifetime normal to the torus equatorial plane is not present in the one-dimensional lifetime profile. The intensity of the sodium cloud trailing the satellite is clearly overestimated by the symmetric (isotropic) emission. The inner hemisphere emission results give a much better match to the observation and suggest that a slight rotation of this emission surface toward the leading hemisphere may contribute the missing outer 500 Rayleigh contour.

Comparison of the observation and model results in Figure 16 therefore suggests that the D_2 intensity of the forward cloud is basically compatible if sodium is assumed to be emitted from the inner hemisphere with a flux of 5×10^9 atoms cm^{-2} sec^{-1}. This represents a flux enhancement of a factor of 50 over earlier flux estimates (see Section 3.2; also, Smyth and McElroy, 1978), which were derived without consideration of the plasma torus. Comparisons of observations and model results for a satellite phase angle near 70 degrees, however, require a smaller flux enhancement factor of about 10.

Model calculations, on the other hand, also indicate that the presence of the plasma torus reduces the column density of sodium seen at Io through the slit (see Figure 3) of Bergstralh et al. (1975, 1977) by only a factor of about 2 to 3. When increased by a factor of 10 to 50, the resulting Bergstralh intensity is too bright and suggests that there is

likely an incompatibility between a strong plasma torus sink for sodium and the observed earth-based sodium intensity measurements. The strength of the sink in Figure 15 therefore appears to be overestimated. This overestimation could result from the assumption, adopted in Figure 15, that the electron and ion temperatures are the same. If so, this suggests that the electron temperature in the hot torus may be significantly less than the ion temperature and that the sodium data may be highly diagnostic in this regard. This will be investigated in our future modeling efforts.

The sodium cloud atoms, upon ionization provide an ion source for the Jovian magnetosphere. The spatial nature of the sodium lifetime, determined by the hot torus plasma properties, will also determine the spatial nature of the sodium ion source. An average radial ion input rate may be calculated by integrating the local ionization rate over the angular and vertical dimensions of the cloud. This radial ion input rate profile for the two model calculations of Figure 16 is given in Figure 17. For sodium emitted from the inner satellite exosphere, see Figure 17a, the ion source is strongly peaked near Io with a maximum value of 6.76×10^{26} ions sec^{-1} in the radial interval 5.8 to 5.9 R_J (Jupiter radii). Note that most of the ions are confined radially with Io's orbit as would be anticipated for this emission surface. The presence of the plasma torus boundary at 5.3 R_J is evident. The radial ion input rate profile for symmetric satellite emission, given in Figure 17b, is essentially unchanged

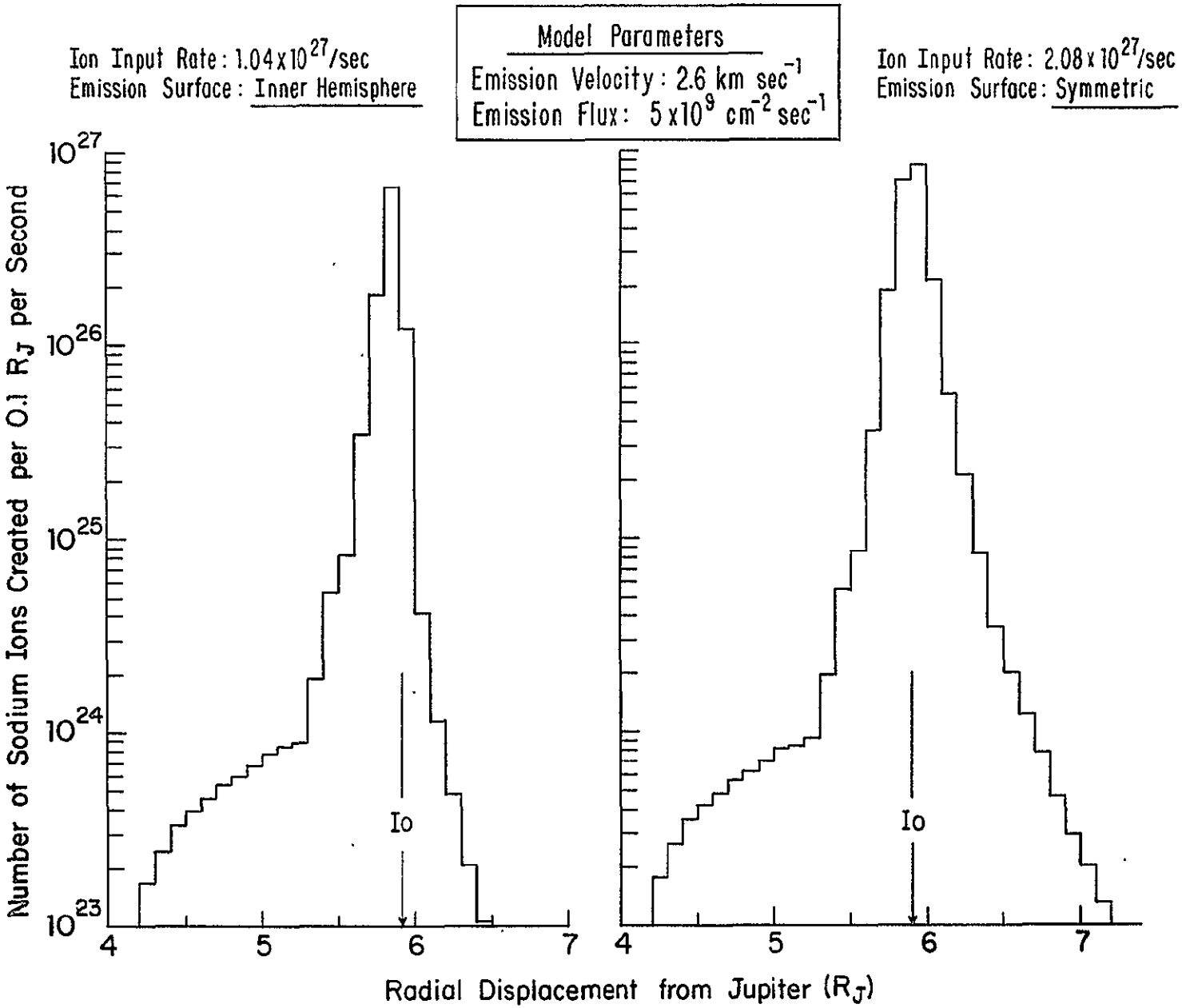

Figure 17. Sodium Ion Source Profile. Calculated radial profiles for the creation rate of sodium ions, based upon the lifetime model of Figure 15, are shown for two different assumed emission surfaces. See text for discussion.

inside of Io's orbit. The addition of the outer hemisphere emission populates the region radially outward from the satellite orbit, and ions, for this calculation, are completely confined within the outer plasma torus boundary (see Figure 15) located at 8.5 R_J.

The ion source rate profiles given in Figure 17 assumed a satellite atom emission flux of 5×10^9 cm^{-2} sec^{-1}. This flux value, as discussed earlier, is likely too large. An independent method of checking this flux value may be provided by evaluating the impact of these ions upon the local electron population. In order to sustain this ion source rate, electrons of sufficient energy must be supplied at a sufficiently large rate. If either the local electron temperature becomes too low through cooling or the local replenishing rate of hot electrons is too small to keep pace with the sodium atoms supply rate, the lifetime of sodium atoms will increase locally and the need to enhance the sodium emission flux to 5×10^9 cm^{-2} sec^{-1} will no longer exist. By this means a lower atom emission flux and a weaker plasma-torus sink (compared to that of Figure 15) might then be in balance and so provide a consistent solution to the sodium cloud plasma torus interaction.

CHAPTER V

TITAN'S HYDROGEN TORUS

5.1 Introduction

Titan, the largest satellite of Saturn, is known to have an atmosphere containing large detectable concentrations of CH_4 (Kuiper, 1944) and perhaps H_2 (Trafton 1972, 1975), although more recent measurements (Munch et al., 1977) make the latter detection less certain. Infrared spectra of Titan's atmosphere by Gillett et al. (1973), showing a pronounced peak at 12 μ, also suggest the presence of C_2H_6. Photochemical processes in Titan's atmosphere, in addition to being able to produce C_2H_6 and other heavy hydrocarbons (Strobel, 1974), may also provide large escape fluxes of hydrogen atoms and molecules to the space around Saturn (Hunten, 1973, 1974; Sagan, 1973; Pollack, 1973; McDonough and Brice, 1973).

McDonough and Brice (1973) first noted that most of the hydrogen escaping Titan would be gravitationally bound to Saturn and would form a toroidal shaped gas cloud around the planet. They suggested that this hydrogen torus might be optically detectable from Earth-orbit and estimated its density to be between 1 and 10^3 atoms or molecules cm^{-3}. They also noted that the actual density and spatial distribution of the torus were functions of the Titanian atmospheric escape flux, the radius and temperature of the exosphere, and the size and strength of Saturn's magnetosphere which,

through charged-particle collisions, could provide the dominant loss process for hydrogen.

A marginal detection of Titan's hydrogen torus was made in 1976 and 1977 and reported by Barker (1977) and Barker et al. (1980) from Lyman-α data obtained from the Earth-orbiting Copernicus satellite. These measurements suggest a Lyman-α brightness of about 200 ±100 Rayleighs resulting from resonance scattering of sunlight by torus hydrogen atoms. Recently a positive detection of the Titan-associated H cloud was reported by Judge et al. (1980) from Lyman-α data obtained by the ultraviolet photometer aboard the Pioneer 11 spacecraft during its encounter with Saturn. The Pioneer 11 measurements indicate that the vertical extent of the cloud is about 1.5 Saturn radii above and below the satellite plane, while the angular extent of the cloud along the satellite orbit is at least 5 Saturn radii from Titan's disk. A complete H torus may exist at a weaker signal, but the limited data precluded a more definitive statement on the angular extent of the cloud. The absolute Lyman-α intensity of the measurements is difficult to determine due to sensitivity changes in the instrument during the encounter, but a preliminary estimate of 100 Rayleighs has been given (Judge et al., 1979).

5.2 Comparison of Models and Pioneer 11 Data

Preliminary models for Titan's hydrogen torus were reported in an earlier NASA report (Smyth, 1978). Key input

parameters for the model were (1) the lifetime of hydrogen atoms in the Saturn environment, (2) the escape flux of hydrogen from the satellite, (3) the exosphere radius and (4) the mean satellite emission velocity. These parameters will be briefly reviewed in the light of new data acquired by the Pioneer 11 spacecraft in its 1979 encounter with Saturn.

In the earlier report, it was assumed that Titan's orbit was wholly contained in the Saturn magnetosphere, which, at Titan's orbit, was assumed to be a corotating plasma with an estimated (Siscoe, 1978) proton density of 1.7 cm^{-3}. This provided a proton flux of 3.4×10^{7} cm^{-2} sec^{-1} and a hydrogen atom charge exchange lifetime of 8.4×10^{6} sec (2300 hours) which dominates the hydrogen photoionization lifetime of $1\text{-}2 \times 10^{9}$ sec. Analysis of the Pioneer 11 data (Smith et al., 1980) has, however, shown that the location of the sunward boundary of the magnetosphere is sensitive to the varying solar wind dynamic pressure and occurred, at times, within the orbit of Titan. When the magnetopause is compressed within the orbit of Titan, the hydrogen lifetime along the unprotected orbit will be characterized by the solar wind plasma having a bulk speed of about 500 km sec^{-1} and a proton density of about 0.2 to 0.3 cm^{-3} (Wolfe et al., 1980). This gives a lifetime of about $5.0\text{-}3.3 \times 10^{7}$ sec. If however the orbit of Titan lies wholly within the magnetosphere, the hydrogen lifetime is determined by the corotating plasma ($\sim$200 km sec^{-1}) with estimated proton density of 0.2-1.0 cm^{-3}

(Frank, 1980) to have a value between 7.1-1.4x10^7 sec. These two estimates of the hydrogen atom lifetime from Pioneer 11 data are of similar magnitude or larger than the earlier estimated value of 8.4x10^6 sec (2300 hours). The earlier lifetime value is sufficient for present purposes and will be adopted for the model calculations.

The escape flux of hydrogen atoms from Titan is controlled by chemistry (Strobel, 1974) and by the processes of vertical transport operative in the atmosphere (Hunter, 1973). A photochemical driven conversion of CH_4 into other heavy hydrocarbons such as C_2H_2, C_2H_4 and C_2H_6 will determine the relative abundance of H and H_2, and suggests (Strobel, 1979) an escape flux ratio H:H_2 in the range 1:9 to 3:7. Assuming an escape flux for both H and H_2 of about 10^{10} cm^{-2} sec^{-1}, based on the satellite surface area, this provides an upper limit H atom escape flux of $3x10^9$ cm^{-2} sec^{-1} and is adopted here for model calculations.

Estimates of the radius of Titan's exosphere range from $4x10^3$ to 10^4 km (Tabarié, 1074) and a nominal value of 5000 km is adopted. A mean emission velocity of 2.0 km sec^{-1} from this exosphere provides the H atoms with sufficient energy so that they escape from the Lagrange sphere of Titan with a characteristic velocity of about 1 km sec^{-1}, a reasonable choice not knowing the thermal characteristics of the upper atmosphere. The emission of hydrogen from the exosphere is assumed to be uniform and isotropic.

Model results showing the column density contour plot of

the toroidal hydrogen cloud of Titan are shown in Figure 18 as seen from above the satellite plane. The cloud shows a fair amount of circular symmetry except near the satellite where the column density is peaked. The orbital-angular extent of hydrogen from Titan of 5 Saturn radii, observed by Pioneer 11 (Judge et al., 1980), is also indicated in Figure 18 and corresponds approximately to the enhanced angular column density peak. This suggests that the UV photometer aboard the Pioneer Saturn spacecraft may have seen only the brighter portion of the H-cloud near the satellite source. This enhanced column density region, more obvious for smaller lifetimes as is illustrated in Figure 19 and Figure 20, will eventually diminish and become part of a cylindrically symmetric torus for lifetimes significantly longer than 2300 hours adopted value.

The earth-orbiting Copernicus satellite viewed the hydrogen torus more nearly in the satellite plane as shown in Figure 21, where Lyman-α intensity contours, assuming solar resonance scattering, are plotted. The total vertical extent of 3 Saturn radii, suggested by Pioneer 11 UV photometer measurements, is also indicated. The cloud intensity near either of the satellite orbit elongation points in Figure 21 is of order 150 to 200 Rayleighs, in good agreement with the Copernicus observations (Barker et al., 1980). During the best Pioneer 11 observation of the near Titan cloud, the spacecraft was, however, inside of Titan's orbit and the line of sight of the UV photometer was non-radial

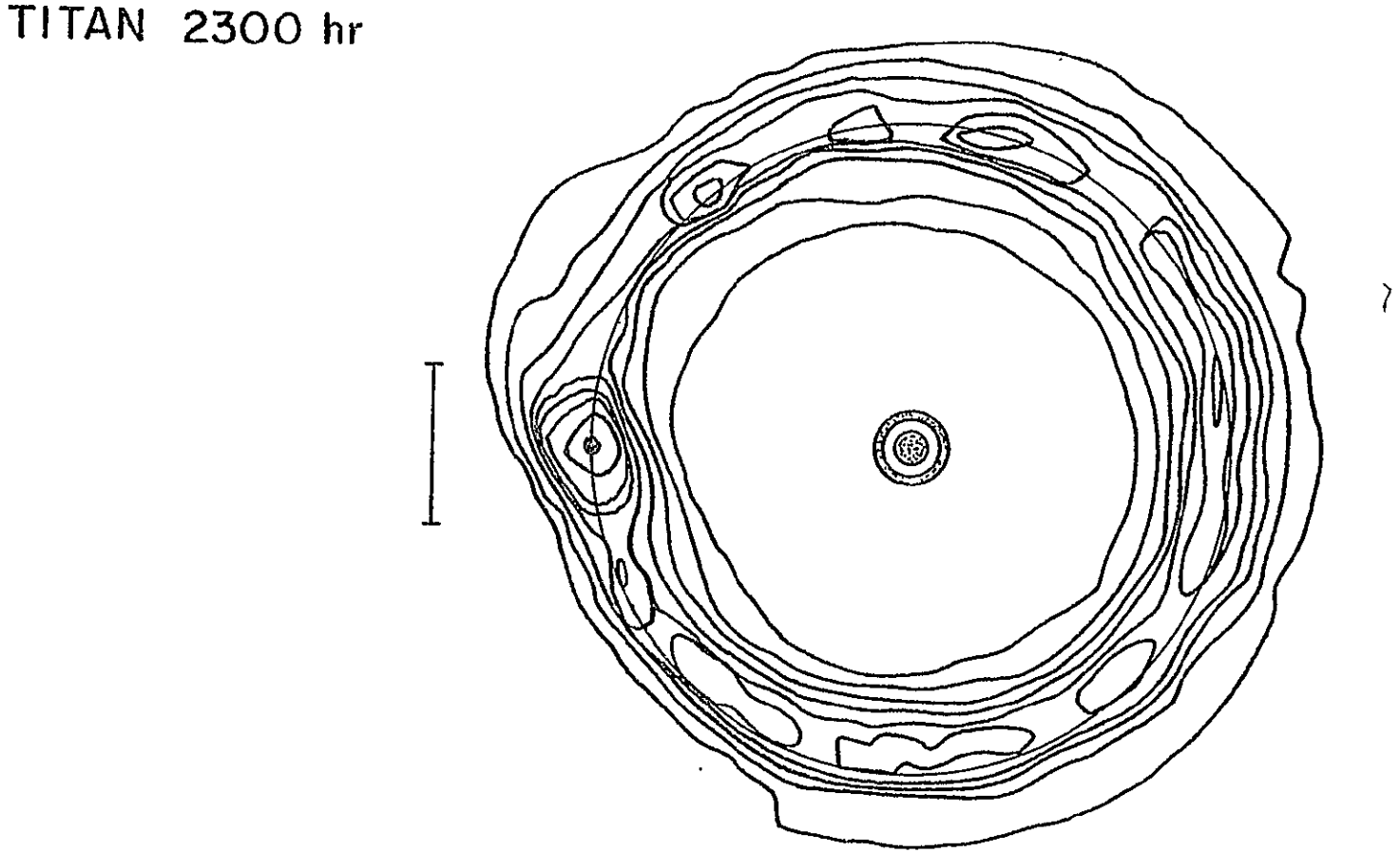

Figure 18. Hydrogen Torus of Titan. Column density contours, calculated from the cloud model for a 2.0 km/sec emission velocity and the indicated lifetime, are shown as viewed from above the satellite plane.

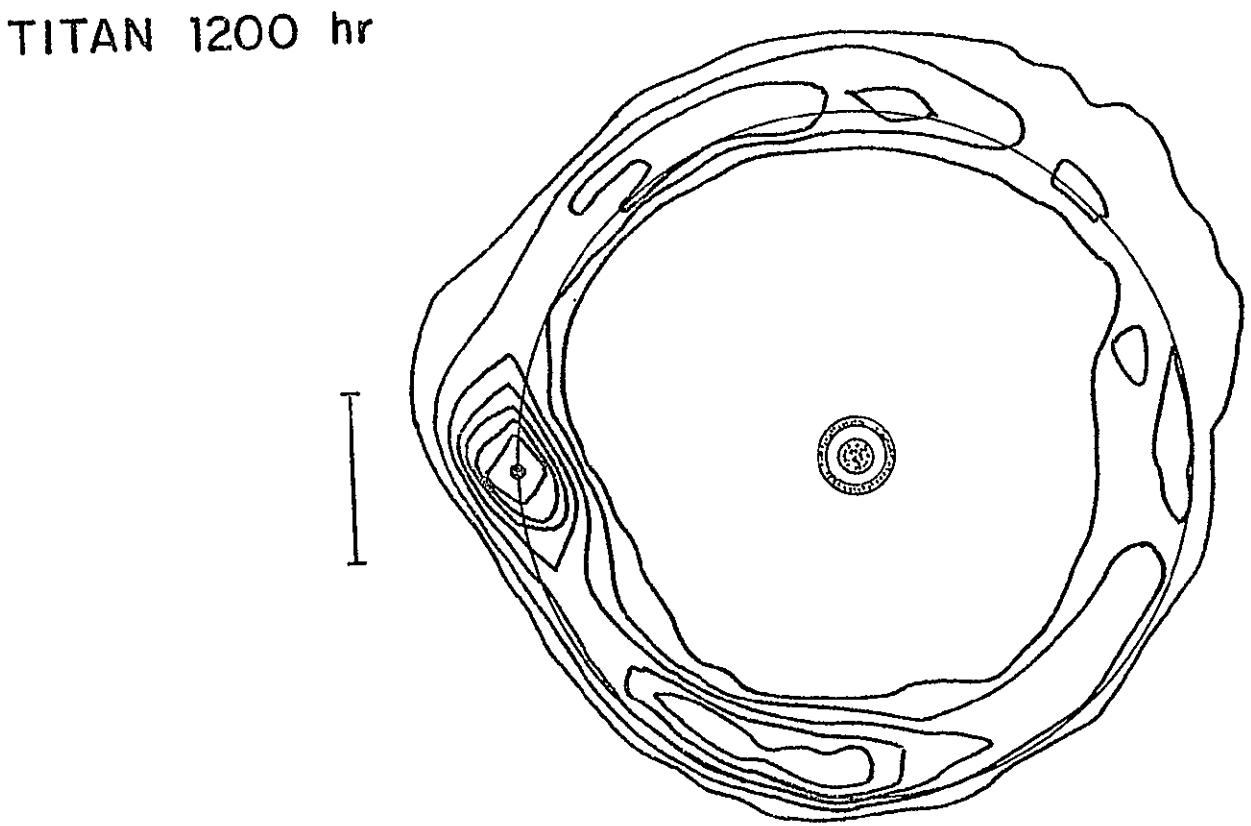

Figure 19. Hydrogen Torus of Titan. Same description as Figure 18.

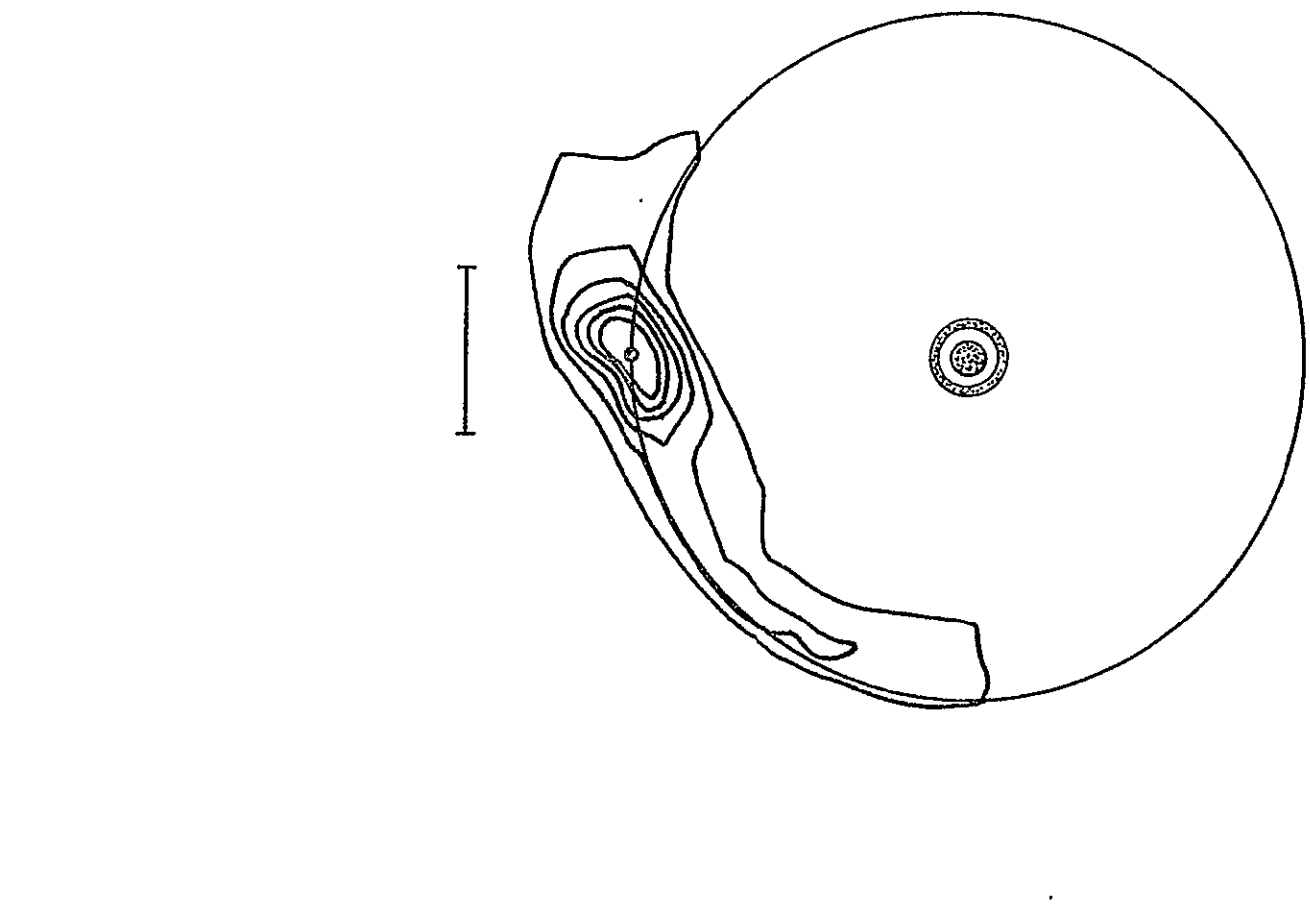

Figure 20. Hydrogen Torus of Titan. Same description as Figure 18.

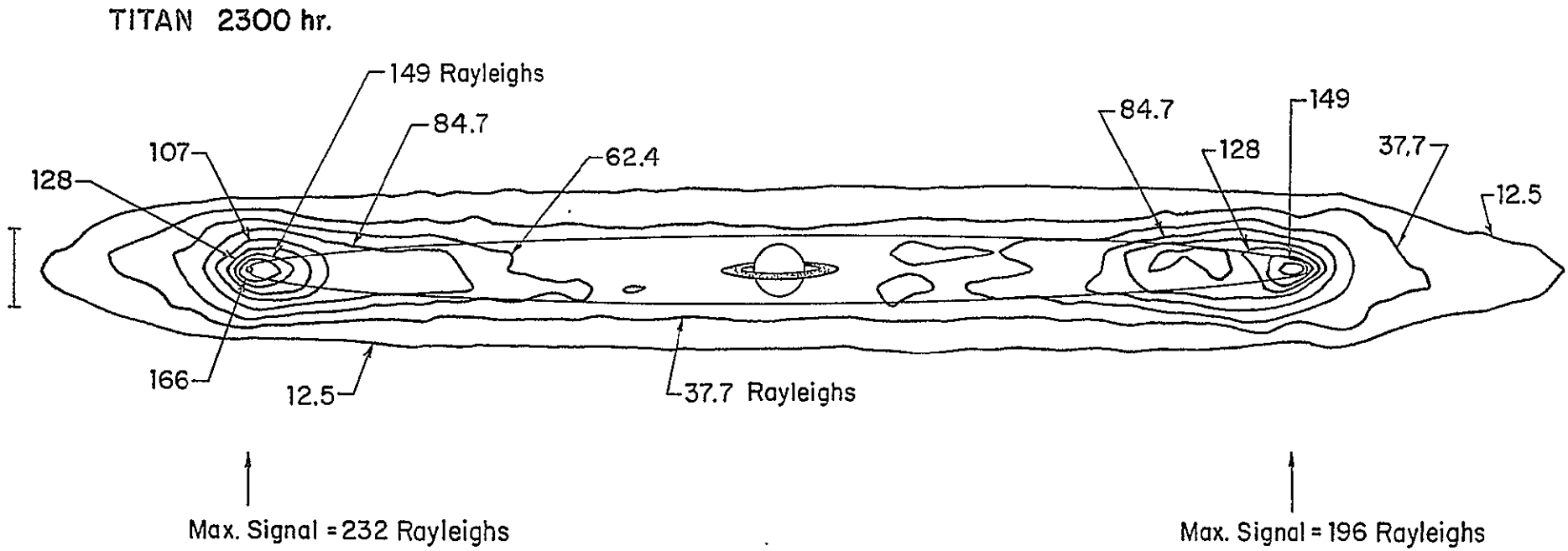

Figure 21. Lyman-α Intensity of Titan's Hydrogen Torus. Intensity contours, calculated assuming resonance scattering of sunlight and the indicated model parameters, are shown for the satellite plane tilted by 3.254 degrees.

(Judge et al., 1980). This viewing perspective would reduce the column density and hence the observed intensity near the elongation point by a factor of 1.5 to perhaps 2, resulting in a maximum observed Pioneer 11 signal of 75 to 130 Rayleighs. This is in excellent agreement with the 100 Rayleigh estimate given by Judge et al. (1979).

In the event that the lifetime of hydrogen atoms near Titan's orbit was smaller than the 2300 hour estimate, a partial toroidal cloud could exist. This is illustrated in Figure 22 and Figure 23 for a lifetime of 1200 hours and 400 hours respectively and might occur if plasma densities were sufficiently enhanced by solar wind compression. If however, the H atoms live longer than the 2300 hour estimate of Figure 21, the hydrogen cloud would be brighter, approximately in proportion to the increased lifetime value.

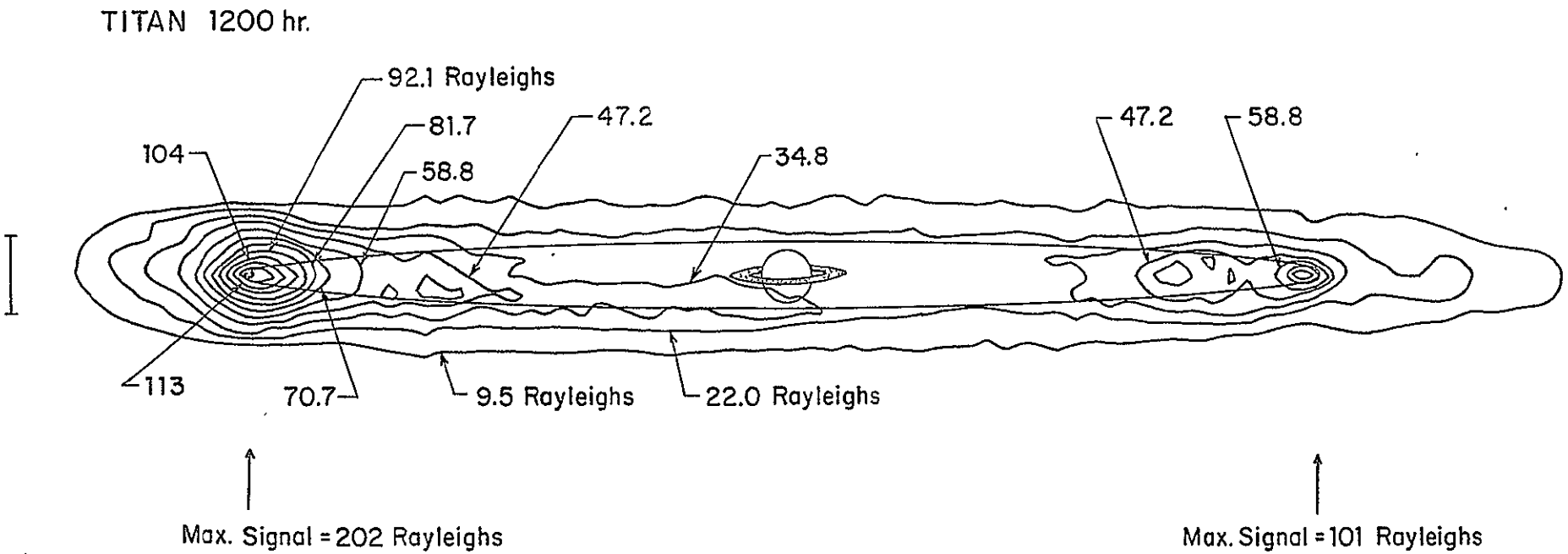

Figure 22. Lyman-α Intensity of Titan's Hydrogen Torus.
Same description as Figure 21.

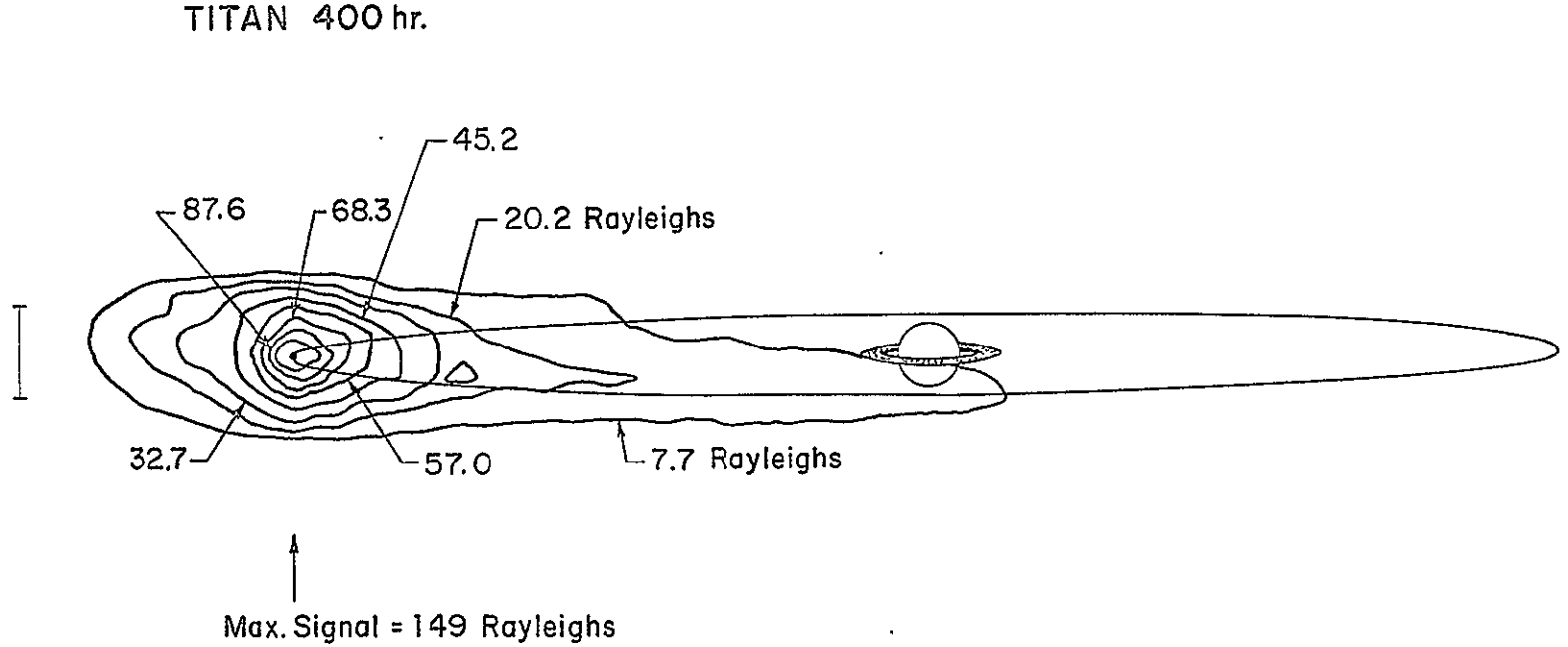

Figure 23. Lyman-α Intensity of Titan's Hydrogen Torus.
Same description as Figure 21.

CHAPTER VI

THE EXTENDED ATMOSPHERES OF COMETS

6.1 Introduction

Interest in studying comets has grown with the realization that understanding the chemical nature and physical structure of the cometary nucleus will advance our understanding of basic physical and chemical processes in cosmogony, molecular astronomy and space physics. The key to understanding the composition, chemistry and structure of the cometary nucleus comes through an examination of the extended atmospheres of comets. It is then clear that supporting research for theoretical modeling of the physical conditions and processes in cometary atmospheres is of considerable importance and will play a definite role in the planning and evaluation of future NASA cometary missions.

The broadening of our scope of research to include cometary atmospheres is a natural extension of our previous modeling of extended satellite atmospheres, since the neutral gas and dust atmospheres of comets may be treated in a similar fashion. Large outer satellites and comets actually represent two extreme cases of solar system bodies which may have extended atmospheres. The large satellites are sufficiently massive that the scale height of a light atmospheric gas such as hydrogen is nearly equal to the satellite radius, so that gravitational escape and formation of an extended atmosphere is just thermally possible. Comets,

on the other hand, with their small size and mass, have enormously large hydrogen scale heights compared to their radius, and cannot retain molecules released from their nucleus by solar heating when near the sun. Comets, therefore, create an atmosphere which is by nature always extended. Solar system objects with sizes immediate to the large satellites and comets may also have extended atmospheres if a source of gaseous material is available from their surfaces.

For descriptive purposes a comet may be divided into three parts: (1) the central solid core or nucleus, (2) the surrounding large gas-like envelope or coma, and (3) the elongated dust and plasma tails. The cometary nucleus is viewed as a solid body consisting of a mixture of ices and rocky material of about 1 to 10 km in diameter. The nucleus moves along a trajectory about the sun and near the sun solar heating of its surface cause the release of icy grains, dust grains and gases. Ejection of this material from the nucelus may not be isotropic because of non-uniform distributions of icy materials on the nucleus, or because of the orientation of the spin axis of the nucleus relative to the sun-comet line.

The icy grains released form the nucleus are basically thought to be snow of clathrate hydrates of gases and may contain considerable concentrations of radical gas species in addition to more chemically stable molecules forming ices. The icy grains, evaporating as they flow away from the nucleus, release the more stable molecules (called

mother or parent molecules) and the radical gas species, thereby providing an extended gas source for the coma. Gas phase reactions between the radical and stable species may then take place. As the gas-ice-dust mixture expands and becomes more optically thin, photochemical reactions also dissociate the parent molecules, releasing daughter molecules which further react through gas phase chemistry.

Gas phase reactions in the coma cease when the gas has expanded sufficiently so that collisions are no longer operative. This defines a boundary for the inner coma which is about 10^4 to 10^5 km in radius. Neutral gas and dust outside of this boundary follow trajectories determined by their initial location and velocity upon emerging and by the forces of solar gravity and solar radiation pressure. This collisionless outflow of gases and dust forms the outer coma and, in the case of atomic hydrogen, has been detected as far as 3×10^7 km from the nucleus. Icy grains may also populate the outer coma. Molecules in the outer coma may be dissociated by sunlight and by this process produce an extended source for the product gas species. Gases are lost from the outer coma by ionization through interaction with solar protons and solar wind particles. Plasma thus formed and dust emerging from the outer coma produce the cometary tails.

The extended gaseous atmospheres of comets may therefore be divided into two parts: the inner coma and the outer coma. Each part of the atmosphere has received considerable

theoretical investigation. Hydrodynamic models have been constructed to describe the outward flow in the inner coma, since in this region intermolecular collisions dominate. Exospheric models, based on collision-free trajectories of gas atoms and molecules, have been developed to describe the flow in the outer coma. The thrust of this research effort is to develop improved exospheric models with sufficient flexibility and accuracy for useful analysis and interpretation of cometary data.

6.2 Description of the Model

The general exospheric model under development is based upon exact orbit calculations in three dimensions and is suitable for interpretative analysis of both the dust and neutral gaseous components of extended cometary atmospheres. The exospheric model is being constructed so as to be capable of modeling a variety of conditions describing the nature of the gas (or dust) source. The cometary source may be specified as either a simple point source or as an extended source. In the latter case the extended source surface could be chosen to coincide with the inner coma boundary upon which the dispersion and anisotropic character of the outflowing gas (or dust) velocity deduced by an inner coma hydrodynamic model, could be used as the initial conditions for the exospheric model. This would provide comprehensive modeling for the complete coma.

In calculating trajectories of the gas (or dust) particles,

the completed model will include the effect of the comet motion, the solar gravitational force and the solar radiation pressure in its entirety. The radiation pressure depends upon the sun-particle distance (intensity and hence pressure decreases with distance), the nucleus-particle distance (near the nucleus optical thickness decreases and radiation pressure increases with distance) and the sun-particle radial velocity (determining the doppler shift and hence the solar intensity seen in the absorption feature as in the case of Lyman-α for a hydrogen atom). The effect of time and heliocentric distance dependence of the production rate of gas (or dust) by the nucleus and the effect of a finite lifetime of gas molecules or atoms along their trajectories may also be included in calculating the coma density.

The completed exospheric trajectory model will be capable of predicting the density, column density and intensity of the coma for arbitrary viewing geometry and as a function of heliocentric distance for given source and lifetime conditions. Line profile shapes of radiation emitted by gases that resonantly scatter sunlight could also be calculated and compared with data to better understand the velocity structure of the coma. The model should be useful both in refinement of analysis of past cometary data and in investigation of new data anticipated in future studies of comets.

The model development has been divided into two phases. The first phase reported here, has emphasized the character-

ization of the orbital mechanics required to describe the motion of gas or dust in the extended comet atmosphere and the numerical methods required to solve these equations efficiently. Included also are preliminary model calculations. The second phase, to be implemented in the coming year, is an improvement and refinement of this basic model in order to incorporate the flexibilities and options discussed above.

6.3 Model Development

The first phase of development of the general exospheric model for extended comet atmospheres, discussed in Section 6.2, is reported. The primary emphasis has been to characterize the orbital mechanics and numerical methods required to describe the motion of gas or dust in the extended comet atmosphere and to perform very preliminary modeling calculations.

The cometary mass is so small that all gas or dust particles escaping from the nucleus or the extended exosphere of the coma (with even thermal gas flow velocities) are negligibly influenced by the gravitational field of the comet. Under these circumstances the motion of the gas or dust particle relative to the sun may be adequately described by the modified Kepler equation for the relative separation vector $\vec{r}$:

$$\ddot{\vec{r}} = -\mu \frac{\vec{r}}{r^3} \quad . \qquad (6.3.1)$$

Here $\ddot{\vec{r}}$ denotes the relative separation acceleration, r the magnitude of the separation distance $\vec{r}$, and

$$\mu = G\bar{M} \quad , \tag{6.3.2}$$

where G is the gravitation constant and $\bar{M}$ is the effective mass of the sun.

The force of solar radiation pressure on the gas or dust reduces the actual solar mass M seen by the comet nucleus to an effective solar mass $\bar{M}$ seen by the gas or dust particle. In particular

$$\bar{M} = M - S/G \tag{6.3.3}$$

where S/r^2 is the average solar radiation acceleration experienced by the gas or dust. For certain gases such as hydrogen and sodium, S may be a function of the radial velocity between the sun and the atom or molecule, while for other gases S may be considered to be constant. For certain gas atoms or dust particles, S is sufficiently large that $\bar{M}$ may be negative (Burns et al., 1979).

The model to determine the spatial distribution of the extended cometary gas or dust atmosphere is based upon solving equation (6.3.1) for an ensemble of gas or dust particles emitted from the comet nucleus, or more generally from the coma exosphere. When S is a constant, solutions to (6.3.1) are the well-known two-body Keplerian orbits. Numerical

exploration has shown that application of Runge-Kutta formulas to equation (6.3.1) provides both a general and efficient method for determining r and $\dot{\vec{r}}$ at time t given r_o and $\dot{\vec{r}}_o$ at an earlier time t_o. Other methods, such as those discussed by Goodyear (1965), are applicable when S is a constant but are not necessarily more efficient in this context.

Model calculations for comet Halley are shown in Figure 24 and illustrate the shape and relative density of hypothetical extended hydrogen atmospheres viewed normal to the comet orbit plane. The density-dot plots are shown for five comet locations chosen symmetrically about the perihelion point. The model is simple, assuming isotropic emission of H atoms from a moving comet point source with initial atom velocities of 8.2 km sec^{-1} and a hydrogen lifetime of 2.2×10^6 sec. The solar radiation acceleration is assumed independent of the sun-atom radial velocity, having an active sun value of 0.7706 cm^{-2} sec^{-1} at 1 AU. This provides an effective solar mass $\bar{M}$ which is both constant and negative, with a magnitude of 0.3 times the real solar mass M. The comet orbit and sun disk are shown approximately to scale in Figure 24, while the comet's extended atmosphere is magnified by a factor of four for enhanced viewing. The clockwise orbit motion of comet Halley introduces an asymmetry in the hydrogen density distribution for symmetrically compared comet locations about perihelion and also determines the direction of curvature of the comet tail.

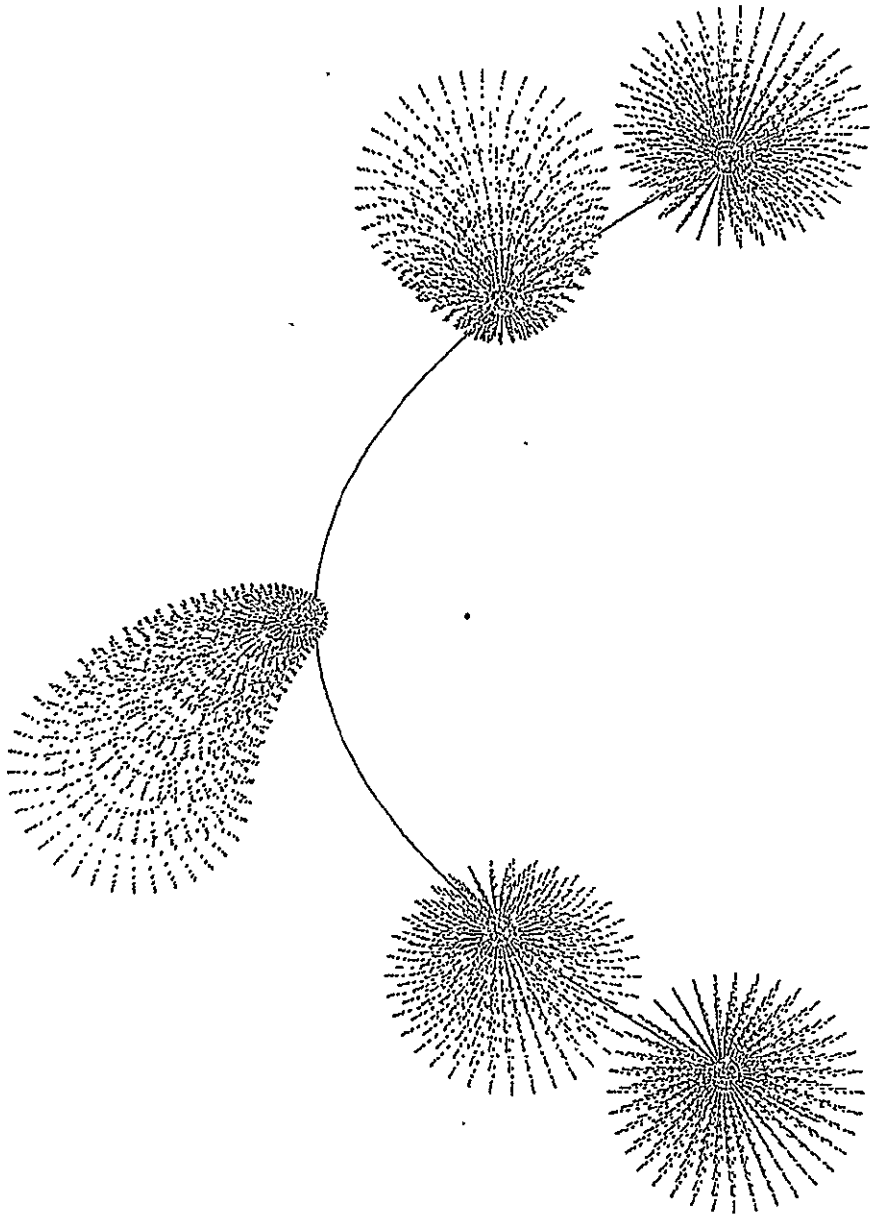

Figure 24. Hydrogen Atmosphere for Comet Halley. Model results of a hypothetical hydrogen atmosphere are shown for a viewing perspective normal to the comet orbit plane. See text for discussion.

Model calculations for comet West are shown in Figure 25 and Figure 26 and illustrate the shape and time evolution of an extended dust atmosphere or tail. The dust tails in Figure 25 are scaled to only half their real size, while the dust tails in Figure 26 are magnified by a factor of four for enhanced viewing. Isotropic emission of dust from the comet nuclei at 1 km sec^{-1} is assumed in both cases, while the lifetime of the dust has a value of $2x10^6$ sec in Figure 25 and $1x10^6$ sec in Figure 26. The strength of the solar radiation pressure in Figure 25 and Figure 26 is chosen to provide an effective solar mass for the dust particles, respectively, of 0.5 and 0.7 times the actual solar mass.

Comet West comes very close to the Sun, having a perihelion distance of only 0.1966 AU. The comet orbit is essentially parabolic, having an eccentricity of 0.99997 and a perihelion velocity of almost 100 km sec^{-1}. Such high velocities and the clockwise motion of the comet give rise to the large curvature of the comet tail shown and to the dramatic change in size of the dust tail before and after perihelion.

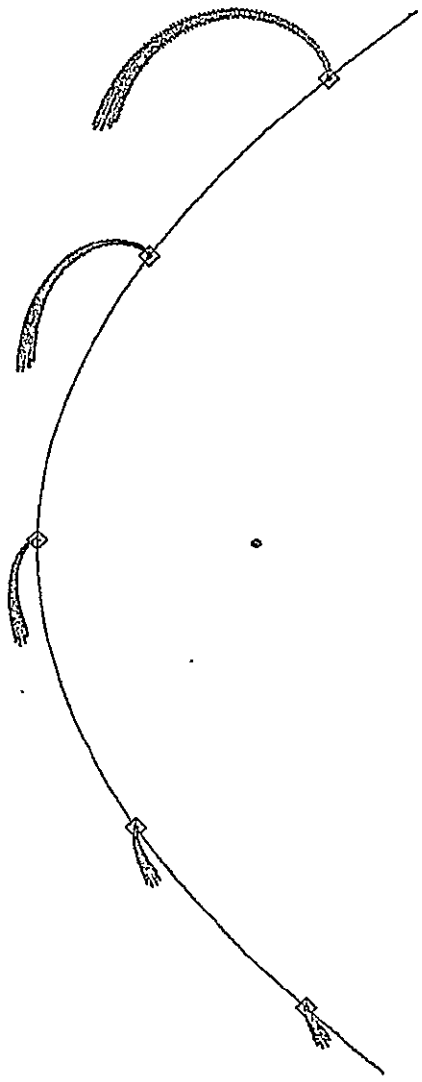

Figure 25. Dust Tail of Comet West.
The space-time evolution of the dust tail, viewed normal to the comet orbit plane, is calculated using the simple comet model described in the text.

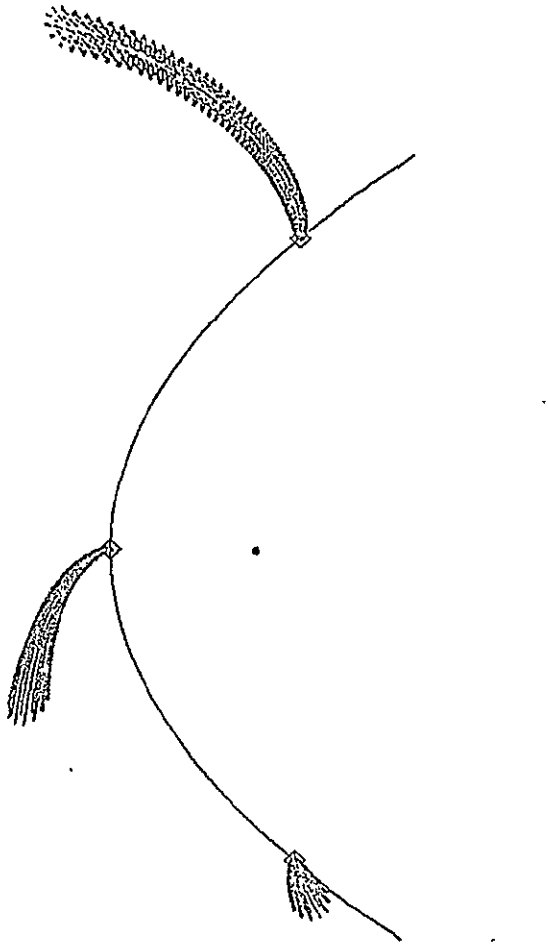

Figure 26. Dust Tail of Comet West.
Same description as Figure 25.

CHAPTER VII

CONCLUDING REMARKS

7.1 Summary

Three different subjects have been discussed in the previous chapters: Io's sodium cloud, Titan's hydrogen torus and the dust and gas atmospheres of comets. A brief summary of the key results of each chapter will follow. In some cases only preliminary or very preliminary results are given and are provided to indicate the state of our current research.

The focus of Chapter II provided quantitative modeling of the sodium cloud to test the hypothesis that solar radiation pressure is the mechanism responsible for the observed east-west asymmetries. The review of observational data indicated that two such asymmetries exist: the Goldberg phase lag asymmetry and the Bergstralh intensity asymmetry. Our earlier modeling effort, in the Appendix, argued more qualitatively for the hypothesis, while more recent results in this chapter provided quantitative calculations based on the three-dimensional model. These model calculations are in excellent agreement with the east-west Goldberg phase lag asymmetry data, predicting not only the correct phase lag but also the correct critical satellite phase angles for observing the cloud symmetrically about Io. Model results also provided an explanation for the east-west Bergstralh intensity asymmetry. This explanation depends critically

upon the presence of low velocity components ($\sim$2 km sec^{-1}) in the actual initial velocity distribution of sodium atoms emitted by the satellite. Assuming the presence of these low velocity components, the maximum observed Bergstralh intensity is matched by the model for an emission flux of about $1x10^{8}$ cm^{-2} sec^{-1}. This value is in agreement with independent estimates of the emission flux deduced by comparison of model calculations and observed two-dimensional sodium cloud images.

Chapter III presents preliminary modeling for the shape of the line profiles of the sodium D-line emission. To initiate the study, line profiles were generated using the monoenergetic model calculations of Chapter II. These line profiles were then compared with observations in order to refine the earlier assumption of monoenergetic emission. Review of observations showed that the line profiles are characterized by a peak and an asymmetrically attached extension or skirt. Monoenergetic model calculations, emitting sodium from the inner satellite hemisphere with a characteristic emission velocity of 2.6 km sec^{-1}, exhibited similar peaks and skirts for satellite phase angles up to about 60 degrees in the east and 240 degrees in the west. For larger phase angles, the absence of the skirt in the model and the presence of the skirt in observational data indicate that an additional emission surface with higher velocity components must be added to the simple monoenergetic model. These higher velocity components must be

emitted approximately tangential to the satellite orbit and have emission speeds of order 15 km sec^{-1}. This suggests that the high speed sodium atoms may be produced by the Jupiter magnetospheric wind interacting with the local Io atmosphere.

In Chapter IV, very preliminary modeling results and speculative ideas regarding the interaction of the sodium cloud and the hot Io plasma torus are discussed. The hot plasma torus, centered on the centrifugal equator at Io's orbital distance, has a radius of approximately one Jupiter radius. The torus may provide a strong sink for ionization of sodium cloud atoms through electron impact. Sodium lifetimes as short as one hour have been suggested and are in marked contrast to values of order 20 hours adopted by earlier modeling of the overall cloud shape and intensity. Such a strong sodium sink, however, would produce an intensity gradient in the sodium cloud, increasing rapidly in brightness toward the satellite. Measurements of the sodium intensity both near Io and in the far sodium cloud, however, constrain this gradient and hence the strength of the lifetime sink. Preliminary model calculations, using this constraint, indicate that the sodium lifetime is likely larger than one hour and hence suggest the presence of a weaker lifetime sink.

Chapter V presents a model for the hydrogen torus of Titan. The torus is complete and exhibits a fair amount of circular symmetry except near the satellite where the cloud

density is peaked. The Lyman-α intensity of the torus, produced by resonance scattering of sunlight, is calculated and compared both with the recent Pioneer 11 measurement and the earlier earth-orbiting measurements of the Copernicus satellite. Agreement with both observations is found for an H atom escape flux from Titan of about 3×10^{9} cm^{-2} sec^{-1}.

In Chapter VI, a new research topic is introduced - the modeling of extended atmospheres of comets. This may be viewed as a natural extension of our satellite atmosphere models, since similar techniques may be employed. The essential features of a comet are reviewed in Section 6.1 and the description of a comet model is discussed in Section 6.2. The first phase of model development, described in Section 6.3, emphasizes the orbital mechanics and numerical methods to be employed for both extended dust and gas atmospheres. Simple model calculations, illustrating the shape and time evolution of the comet atmosphere, are given for comet Halley and comet West.

7.2 Future Emphasis and Direction

Understanding the processes by which gases escape from Io will continue to be an important goal in our research program. The discovery of the hot plasma torus by Voyager 1, with its large flux of sulfur and oxygen ions, indicates that SO_2 (or its chemical fragments) in Io's bound atmosphere is escaping with a flux in excess of the sodium escape flux.

Understanding the escape of sodium from Io is therefore important in a larger context.

Key to understanding the escape of sodium from Io is the determination of the initial atom velocity distribution operative at the satellite. Information about this velocity distribution is contained in the sodium cloud data. The east-west Bergstralh intensity asymmetry data are sensitive to the very low velocity components, while the line profile data are sensitive to the high velocity components. The two-dimensional sodium cloud image data are sensitive to the intermediate velocity components. Future research should be directed to unlocking the velocity distribution from these data. In order to be successful, this process cannot be achieved independently, but must include additional factors, such as understanding the impact of the plasma torus on the sodium cloud. A comprehensive modeling program is therefore required.

Understanding the Jovian magnetosphere and its interactions with Io and with Jupiter are also important goals of our research. The rates at which ions, supplied by gases escaping Io, diffuse from the plasma torus to the larger magnetosphere, and the energy balances which operate in the magnetosphere to maintain the plasma torus are both topics of current interest. Modeling of the sodium cloud data may be helpful in both of these regards also. The sodium ion input rate to the magnetosphere may be calculated by the model and compared directly, by solving the ion diffusion

problem, with Voyager ion data. Such a comparison may be able to define or constrain the ion diffusion coefficients. In addition modeling of sodium cloud properties can provide important constraints upon the electron energy and number density profiles in the hot plasma torus as discussed in Section 7.1. Such constraints are important in understanding the plasma torus energy balance processes. Our future modeling, in cooperation with other disciplined scientists, will pursue these research issues.

In addition to the above research topics for the Jupiter system, our future modeling interest for the Saturn system will continue to increase. The encounter of Voyager 1 with Saturn later this year should provide improved data for Titan and also provide more data for a possible extended hydrogen atmosphere associated with the planetary rings. In addition to this ring atmosphere, a gas torus supplied by several inner satellites of Saturn may also be presented as is suggested by Pioneer 11 measurements indicating a dense, hot plasma located between 4 and 8 planetary radii. Modeling for the ring atmosphere and its role as an ion source for the inner magnetosphere of Saturn will be initiated. Improved modeling of Titan's hydrogen torus will also be considered.

Finally, future comet modeling will continue and emphasize the refinement of the simple model developed under phase one. This will require adding flexibilities to the model code so that it may be more easily applied directly to cometary data.

ACKNOWLEDGEMENT

Computer time for model calculations provided by the National Center for Atmospheric Research, which is sponsored by the National Science Foundation, is gratefully acknowledged.

REFERENCES

Bagenal, F., Sullivan, J.D. and Siscoe, G.L., "Spatial Distribution of Plasma in the Io Torus." Geophys. Res. Lett., 7, 41 (1980).

Barker, E. S., "Progress Report: Copernicus Observations of Solar System Objects." Presented at the 8th Annual Meeting of the AAS/DPS, January 19-22, 1977, Honolulu, Hawaii.

Barker, E., Cazes, S., Emerich, C., Vidal-Madjar, A. and Owen, T., "Lyman-Alpha Observations in the Vicinity of Saturn with Copernicus." Astrophys. J. submitted (1980).

Bergstralh, J.T., Matson, D.L. and Johnson, T.V., "Sodium D-Line Emission from Io: Synoptic Observations from Table Mountain Observatory." Astrophys. J. (Letters), 195, L131 (1975).

Bergstralh, J.T., Young, J.W., Matson, D.L. and Johnson, T.V., "Sodium D-Line Emission from Io: A Second Year of Synoptic Observation from Table Mountain Observatory." Astrophys. J. (Letters), 211, L51 (1977).

Bridge, H.S., Belcher, J.W., Lazarus, A.J., Sullivan, J.D., McNutt, R.L., Bagenal, F., Scudder, J.D., Sittler, E.C., Siscoe, G.L., Vasyliunas, V.M., Goertz, C.K. and Yeates, C.M., "Plasma Observations Near Jupiter: Initial Results from Voyager 1." Science, 204, 987 (1979).

Broadfoot, A.L., Belton, M.J.S., Takacs, P.Z., Sandel, B.R., Shemansky, D.E., Holberg, J.B., Ajello, J.M., Atreya, S.K., Donahue, T. M., Moos, H.W., Bertaux, J.L., Blamont, J.E., Strobel, D.F., McConnell, J.C., Dalgarno, A., Goody, R. and McElroy, M.B., "Extreme Ultraviolet Observations from Voyager 1 Encounter with Jupiter." Science, 204, 979 (1979).

Brown, R.A., "Optical Line Emission from Io." IAU Symposium No. 65, Exploration of the Planetary System, A. Woszczyk and C. Iwaniszewska (eds), Dordrecht: Reidel, pp. 527-531 (1974).

Brown, R.A., "Measurements of SII Optical Emission from Jupiter's Thermal Plasma." Astrophys. J. (Letters), 224, L97 (1978).

Brown, R.A. and Chaffee, F.H. Jr., "High-Resolution Spectra of Sodium Emission from Io." Astrophys. J. (Letters), 187, L125 (1974).

Burns, J.A., Lamy, P.L. and Soter, S., "Radiation Forces on Small Particles in the Solar System." Icarus, 40, 1 (1979).

Carlson, R.W., Matson, D.L., Johnson, T.V. and Bergstralh, J.T., "Sodium D-Line Emission from Io: Comparison of Observed and Theoretical Line Profiles." Astrophys. J., 223, 1082 (1978).

Frank, L.A., Private communication (1980).

Gillett, F.C., Forrest, W.J. and Merrill, K.M., "8-13 μ Observations of Titan." Astrophys. J. (Letters), 184, L93 (1973).

Goldberg, B.A., Carlson, R.W., Matson, D.L. and Johnson, T.V., Bull. AAS, 10, 579 (1978).

Goldberg, B.A., Mekler, Y.B., Carlson, R.W., Johnson, T.V. and Matson, D.L., "Io Sodium Emission Cloud and the Voyager 1 Encounter." J. Geophys. Res. submitted (1980).

Goodyear, W.H., "A General Method for the Computation of Cartesian Coordinates and Partial Derivatives of the Two-Body Problem." NASA CR-522 (1965).

Hunten, D.M., "The Escape of H_2 from Titan." J. Atmos. Sci., 30, 726 (1973).

Hunten, D.M., "Blowoff and Escape of H_2." The Atmosphere of Titan. NASA SP-340, D.M. Hunten (ed) p. 110 (1974).

Judge, D.L., Wu, F-M. ,and Carlson, R.W., "Pioneer 11 Ultraviolet Photometer Measurements of the Saturnian System." Presentation at the 1979 Fall AGU Meeting, December 3-7, San Francisco, California (1979).

Judge, D.L., Wu, F-M. and Carlson, R.W., "Ultraviolet Photometer Observations of the Saturnian System." Science, 207, 431 (1980).

Kuiper, G.P., "Titan: A Satellite with an Atmosphere." Astrophys. J., 100, 378 (1944).

Kupo, I., Mekler, Y. and Eviatar, A., "Detection of Ionized Sulfur in the Jovian Magnetosphere." Astrophys. J. (Letters), 205, L51 (1976).

Macy, W. and Trafton, L., "The Distribution of Sodium in Io's Cloud: Implications." Icarus, 41, 131 (1980).

Matson, D.L., Goldberg, B.A., Johnson, T.V. and Carlson, R.W., "Images of Io's Sodium Cloud." Science, 199, 531 (1978).

McDonough, T.R. and Brice, N.M., "A Saturnian Gas Ring and the Recycling of Titan's Atmosphere." Icarus, 20, 136 (1973).

Münch, G., Trauger, J.T. and Roesler, F.L., "A Search for the H_2 (3,0) S1 Line in the Spectrum of Titan." Astrophys. J., 216, 963 (1977).

Murcray, F.J., "Observations of Io's Sodium Cloud." Ph.D. Thesis, Physics Department, Harvard University (1978).

Murcray, F.J. and Goody, R.M., "Pictures of the Io Sodium Cloud." Astrophys. J., 226, 327 (1978).

Pilcher, C.B., Private communication (1980).

Pilcher, C.B. and Morgan, J.S. "The Distribution of [SII] Emission Around Jupiter." Astrophys. J. in press (1980).

Pollack, J.B., "Greenhouse Models of the Atmosphere of Titan." Icarus, 19, 43 (1973).

Sagan, C., "The Greenhouse of Titan." Icarus, 18, 649 (1973).

Sandel, B.R., Shemansky, D.E., Broadfoot, A.L., Bertaux, J.L., Blamont, J.E., Belton, M.J.S., Ajello, J.M., Holberg, J.B., Atreya, S.K., Donahue, T.M., Moos, H.W., Strobel, D.F., McConnell, J.C., Dalgarno, A., Goody, R., McElroy, M.B. and Takacs, P.Z., "Extreme Ultraviolet Observatons from Voyager 2 Encounter with Jupiter." Science, 206, 962 (1979).

Scudder, J.D., Private communication (1980).

Siscoe, G.L., "Magnetosphere of Saturn." The Saturn System. NASA CP-2068, Hunten and Morrison (ed) p. 265 (1978).

Smith, E.J., Davis, L., Jones, D.E., Coleman, P.J., Colburn, D.S., Dyal, P. and Sonett, C.P., "Saturn's Magnetic Field and Magnetosphere." Science, 207, 407 (1980).

Smyth, W.H., "Outer Satellite Atmospheres: Their Nature and Planetary Interactions." Final NASA Report for period June-December (1978).

Smyth, W.H., "Io's Sodium Cloud: Explanation of the East-West Asymmetries." Astrophys. J., 234, 1148 (1979).

Smyth, W.H. and McElroy, M.B., "The Sodium and Hydrogen Gas Clouds of Io." Planet. Space Sci., 25, 415 (1977).

Smyth, W.H. and McElroy, M.B., "Io's Sodium Cloud: Comparison of Models and Two-Dimensional Images." Astrophys. J., 226, 336 (1978).

Strobel, D.F., "The Photochemistry of Hydrocarbons in the Atmosphere of Titan." Icarus, 21, 466 (1974).

Strobel, D.F., Private communication (1979).

Tabarié, N., "Atomic Hydrogen Distribution." The Atmosphere of Titan. NASA SP-340, Hunten (ed) p. 123 (1974).

Trafton, L., "On the Possible Detection of H_2 in Titan's Atmosphere." Astrophys. J., 175, 285 (1972).

Trafton, L., Astrophys. J., 195, 805 (1975).

Trafton, L., "High-Resolution Spectra of Io's Sodium Emission." Astrophys. J. (Letters), 202, L107 (1975).

Trafton, L., "Periodic Variation in Io's Sodium and Potassium Clouds." Astrophys. J., 215, 960 (1977).

Trafton, L. and Macy, W. Jr., "An Oscillating Asymmetry to Io's Sodium Emisson Cloud." Astrophys. J. (Letters), 202, L155 (1975).

Trafton, L. and Macy, W. Jr., "Io's Sodium Emission Profiles: Variations Due to Io's Phase and Magnetic Latitude." Astrophys. J., 215, 971 (1977).

Trafton, L. and Macy, W. Jr., "On the Distribution of Sodium in the Vicinity of Io." Icarus, 33, 322 (1978).

Trauger, J., Roesler, F. and Münch, G., Bull. AAS, 8, 468 (1976).

Trauger, J.T., Münch, G. and Roesler, F.L., "A Study of the Jovian [SII] Nebula at High Spectral Resolution." Astrophys. J. in press (1980).

Warwick, J.W., Pearce, J.B., Riddle, A.C., Alexander, J.K., Desch, M.D., Kaiser, M.L., Thierman, J.R., Carr, T.D., Gulkis, S., Boischot, A., Harvey, C.C. and Pederson, B.M., "Voyager 1 Planetary Radio Astronomy Observations near Jupiter." Science, 204, 995 (1979).

Wolfe, J.H., Mihalov, J.D., Collard, H.R., McKibbin, D.D., Frank, L.A. and Intriligator, D.S., "Preliminary Results on the Plasma Environment of Saturn from Pioneer 11 Plasma Analyzer Experiment." Science, 207, 403 (1980).

APPENDIX

C-2

THE ASTROPHYSICAL JOURNAL, 234:1148–1153, 1979 December 15

IO'S SODIUM CLOUD: EXPLANATION OF THE EAST-WEST ASYMMETRIES

WILLIAM H. SMYTH
Atmospheric and Environmental Research, Inc., Cambridge, Massachusetts
Received 1979 June 11; accepted 1979 July 6

ABSTRACT

Ground-based observations accumulated over the last few years have established certain asymmetric features of Io's sodium cloud, when data are compared for symmetrically opposite satellite locations east and west of Jupiter. Asymmetries, occurring both in the absolute intensity and in the intensity distribution of the D_1 and D_2 cloud emissions, have been reported independently. Modeling efforts presented, argue that both of these asymmetries are produced by the perturbing effects of solar radiation pressure on the motion of sodium atoms in the cloud. The resonance scattering of sunlight by sodium cloud atoms, which makes the cloud visible, is therefore also responsible for the observed east-west periodic time variation in the cloud shape and density that is correlated with the satellite phase angle.

Subject headings: planets: Jupiter — planets: satellites

I. INTRODUCTION

Io, the innermost Galilean satellite of Jupiter, is the source of an extended sodium atmosphere emitting radiation in the D_1 and D_2 lines. Discovered by Brown in 1973 (Brown 1974), the cloud has since become the object of many ground-based observations, studying both its spectral and spatial characteristics (Brown and Chaffee 1974; Trafton, Parkinson, and Macy 1974; Mekler and Eviatar 1974; Bergstralh, Matson, and Johnson 1975; Brown *et al.* 1975; Trafton 1975; Trafton and Macy 1975; Macy and Trafton 1975; Wehinger, Wyckoff, and Frolich 1976; Mekler, Eviatar, and Coroniti 1976; Münch, Trauger, and Roesler 1976; Trauger, Roesler, and Münch 1976; Münch and Bergstralh 1977; Bergstralh *et al.* 1977; Goody and Apt 1977; Trafton 1977; Trafton and Macy 1977; Carlson *et al.* 1978; Matson *et al.* 1978; Murcray and Goody 1978; Goldberg *et al.* 1978; Mekler and Eviatar 1978). Attention here will be restricted to better understanding data describing the spatial distribution of the sodium cloud as a function of phase angle.

Models developed to interpret the main spatial features of the sodium cloud have been successful in deducing the lifetime of the neutral gas as well as defining and constraining the range of emission conditions for sodium at the satellite-magnetosphere interface. In early modeling, Carlson, Matson, and Johnson (1975) argued that the lifetime of sodium atoms would be limited by electron impact ionization. They suggested a sodium lifetime between about 30 and 50 hours depending on the plasma conditions prevalent in the Jovian magnetosphere. More recently, Matson *et al.* (1978) presented two images of the cloud, where sodium was seen to precede Io, indicating that sodium atoms were emitted nonisotropically from Io. Smyth and McElroy (1978) extended their earlier model (Smyth and McElroy 1977) to nonisotropic emission and applied it to a set of 56 two-dimensional sodium images reported by Murcray and Goody (1978). They concluded that the neutral lifetime of sodium in the Jovian magnetosphere was between 15 and 20 hours and that the sodium appeared to be ejected primarily from the inner hemisphere of the satellite with a mean velocity of 2.6 km s^{-1} and with an emission source strength of about 2×10^{25} atoms s^{-1}. They also concluded that the sodium cloud precedes Io and furthermore that it is aligned along a central axis tilted approximately 35° toward Jupiter with respect to the line drawn through Io and tangent to the satellite orbit. An illustration taken from their paper showing this orientation of the sodium cloud is given in Figure 1.

The modeling efforts of Smyth and McElroy indicate that the global features of the sodium cloud may, to a first approximation, be treated as a steady state cloud. Observed changes in the intensity pattern of the cloud with satellite phase angle are therefore largely due to the changing geometric viewing perspective of the cloud projected onto the plane of the sky. Small modulations in the steady state intensity of the cloud, occurring in a time of order 2 hours (Trafton 1977), were present in the data of Murcray and Goody (1978). These changes are correlated with the magnetic field and are presumably fluctuations in the ionization lifetime of the sodium atoms.

Other changes in the sodium cloud, occurring when data are compared for satellite orbital phase angles separated by 180°, suggest, however, that the steady state picture of the cloud is not complete and furthermore that a time-varying mechanism is operative, with a period equal to the satellite period. These types of changes are referred to as the east-west asymmetries of the sodium cloud. Two different east-west asymmetries have been observed and are discussed below. A simple physical explanation is presented.

In brief, it will be shown that both east-west

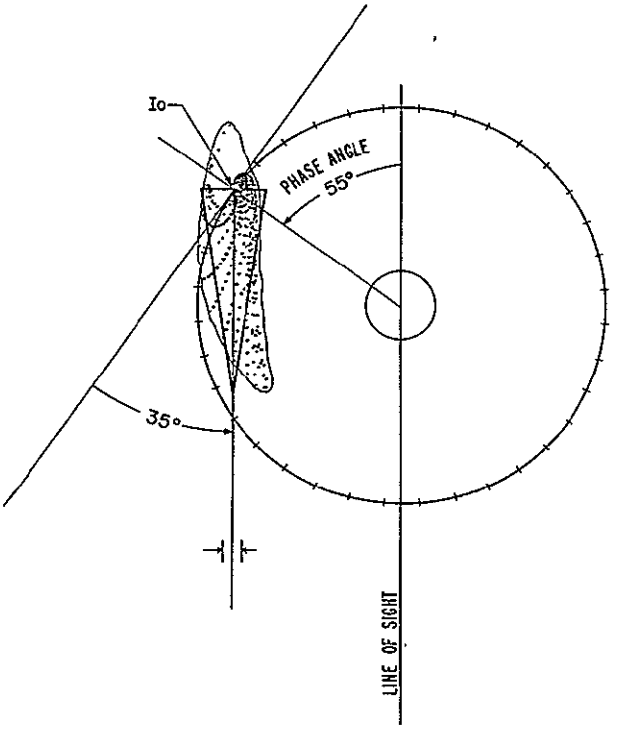

FIG. 1.—Sodium cloud model. The shape of the sodium cloud in the satellite plane calculated by Smyth and McElroy (1978) is shown for a phase angle of 55° and compared with their simple triangular cloud model. An emission velocity of 2.6 km s^{-1} and a lifetime of 20 hours were assumed. Atom concentration is proportional to the density of points shown.

asymmetries follow directly from spatial distortions of the sodium cloud produced by the solar radiation pressure effect of resonance scattering in the D_1 and D_2 lines. Orbit calculations illustrating the time-dependent changes in the sodium atom trajectories produced by the solar radiation force as a function of Io's orbital location are presented in support of this explanation. Detailed three-dimensional calculations of the cloud density and its corresponding two-dimensional intensity pattern are in progress and will be reported at a later date. The ability of solar radiation pressure to distort gravitationally controlled orbits has previously been recognized in several other physical situations, such as the hydrogen comae (Keller and Thomas 1975) and dust tails (Finson and Probstein 1968) of comets, the motion of artificial satellites (Kozai 1961), and the distribution of hydrogen in the upper geocorona (Bertaux and Blamont 1973).

II. THE EAST-WEST ASYMMETRIES

The sodium cloud exhibits two different east-west asymmetries. The first and best documented of these was reported by Bergstralh, Matson, and Johnson (1975). They observed the intensity of the sodium cloud as a function of phase angle through a 3″ × 8″ slit centered on the satellite with the long dimension of the slit oriented approximately perpendicular to the projection of Io's orbital plane. In addition to showing the intensity was correlated with Io's orbital position about Jupiter, and thereby identifying resonance scattering of sunlight by sodium atoms as the dominant excitation mechanism, they also showed that during their 7 week observing period the measured intensity of the cloud with the satellite east of Jupiter was consistently about 50% greater than the measured intensity with the satellite west of Jupiter. In a second article (Bergstralh *et al.* 1977) they reported additional data to increase the original 1974 observing period to 10 weeks and also included observations made during the 1975 apparition. The combined data base strengthened their original conclusions, with an analysis of selected data then establishing the east-west intensity asymmetry more accurately at 20–25%.

The second and more recently discovered east-west asymmetry was reported by Goldberg *et al.* (1978). Their observations showed that the projected intensity pattern of the cloud on the plane of the sky did not produce a mirror image at orbital phase angles separated by 180°. As the satellite approaches either the eastern or western elongation point of its orbit (90° or 270°, respectively), there exists a critical phase angle for which the sodium cloud appears nearly circularly symmetric about Io. For phase angles larger than this critical angle, the sodium cloud has an elongated shape (see Murcray and Goody 1978). The eastern and western critical satellite phase angles for which the cloud exhibits this symmetry were originally reported by Goldberg *et al.* (1978) as 65° and 230°, respectively. More recent estimates made with additional observations (Goldberg 1979) suggest that the critical eastern phase angle is more accurately in the 70°–75° range. This suggests that in the east the central axis of the sodium cloud is tilted only about 15° or 20° with respect to the line drawn tangent to the satellite orbit at Io, whereas in the west the tilt angle is about 40°. The steady state sodium cloud depicted in Figure 1 has a tilt angle of 35°. Although the exact critical phase angle for a symmetric cloud may be difficult to estimate precisely for each cloud image of Goldberg *et al.* (1978) because of the 17°–25° of orbital smear associated with their 2–3 hour long measurements, the east-west asymmetry in the satellite phase angle of order 20°–25° appears to be real. No explanation for this asymmetry has been given.

Possible explanations of the east-west intensity asymmetry reported by Bergstralh *et al.* (1975, 1977) have appealed mainly to time-dependent changes in the sodium source at Io. Bergstralh, Matson, and Johnson (1975) suggested that the asymmetry was due to a nonuniform sodium distribution, perhaps resulting from asymmetrical ejection of sodium from Io. Smyth and McElroy (1977) presented calculations to show that if the sodium atoms seen with Io near western elongation had been emitted with a slightly higher ejection velocity than those seen near eastern elongation, the asymmetry could be achieved. They appealed to the changing sunlit hemisphere of Io and its interaction with the magnetic field as a possible modulation mechanism. In a later paper (Smyth and McElroy

1978), enhancement of the higher components of the sodium initial velocity dispersion when the satellite is near western elongation was also suggested as a possible explanation for a similar east-west intensity asymmetry trend seen in the data of Murcray and Goody (1978). Trafton (1975) took a different approach, suggesting that radial streaming of sodium atoms in the cloud with velocities as high as 18 km s^{-1} might brighten the Io disk component of the intensity at eastern elongation.

An alternative and very simple explanation of both east-west asymmetries will be advanced here. It is based upon the force experienced by sodium atoms as they resonantly scatter sunlight and upon the ability of this force to alter the cloud atom orbits, as determined by the gravitational fields of Io and Jupiter.

III. THE EFFECT OF SOLAR RADIATION PRESSURE

A sodium atom in Io's cloud upon absorbing a photon of energy $h\nu_i$ in either the D_1 line ($\lambda_1 = 5889.95$ Å) or the D_2 line ($\lambda_2 = 5895.92$ Å) will experience in the Sun-Jupiter vector direction a momentum change $h\nu_i/c$ and a corresponding velocity change of about 2.9 cm s^{-1}. The excited atom, returning to its ground state in about 10^{-8} s by resonance emission of a photon, will also experience a second velocity change of the same magnitude along an arbitrary vector direction (neglecting the slightly forward peaked D_2 phase function). The rate J_i at which a sodium atom absorbs photons in the D_1 line ($i = 1$) and the D_2 line ($i = 2$) is given by

$$J_i = \gamma_i(v)\left(\frac{\pi e^2}{m_e c}\right)\frac{(\pi F_{\nu_i})}{h\nu_i} f_i R^{-2}, \qquad (1)$$

where R is the Sun-Jupiter distance in astronomical units, f_i is the oscillator strength of the ith line, πF_{ν_i} is the solar continuum-level photon energy flux between the D_1 and D_2 lines at $R = 1$,

$$(\pi F_{\nu_i}) = 6.80 \times 10^{-5}\frac{\lambda_i^2}{c} F_\lambda' \qquad (2)$$

(see Allen 1976), and $\gamma_i(v)$ is the fraction of this solar continuum flux available to the sodium atom as it is Doppler shifted out of the bottom of the solar D-line Fraunhofer absorption feature by the instantaneous radial velocity v of the sodium atom relative to the Sun. The fraction $\gamma_i(v)$ varies from about 0.05 at the bottom of the solar absorption feature ($v \approx 0$) to about 0.6–0.7 with a velocity v equal to the orbital speed of Io.

For Jupiter at mean opposition ($R = 5.2028$), the time $(J_i)^{-1}$ between absorption of two photons of frequency ν_i varies from a few seconds to many tens of seconds depending upon the value of γ_i and, in any event, is small compared with characteristic times of order 1 hour for orbital motion of a sodium atom in the cloud. Because of this, the randomly directed momentum change of the sodium atom produced by the resonance emission of the photon will average to zero. The net radiation acceleration b experienced by the sodium atom is therefore produced by the initial photon absorptions and is given by

$$b = \frac{1}{m_0}\left(\frac{h\nu_1}{c} J_1 + \frac{h\nu_2}{c} J_2\right). \qquad (3)$$

This acceleration is directed radially outward from the Sun. Here m_0 is the mass of the sodium atom. Evaluating (3) for Jupiter at mean opposition gives

$$b = 0.650(\gamma_1 + 1.996\gamma_2), \qquad (4)$$

where the units are expressed in cm s^{-2}. In comparison, the acceleration experienced by a sodium atom in a circular orbit at Io's orbital radius is only 71.27 cm s^{-2}. The magnitude of the radiation acceleration is therefore as large as 1–2%. This is a significant perturbation and will alter the sodium cloud atom orbits determined by the gravitational accelerations of Io and Jupiter appreciably, as will be demonstrated.

Sodium atoms observed in the cloud at any given time were initially emitted by Io at a somewhat earlier time, corresponding to an earlier phase angle for the satellite. For a sodium lifetime of 20 hours, the longest-lived cloud atoms were actually emitted about 170° earlier—almost at the symmetrically opposite orbital location of the satellite. Distortion in the observed sodium cloud near eastern elongation will therefore be caused by the cumulative effects of the radiation acceleration on atom orbits emitted near western elongation. The distortion in the observed cloud near western elongation will likewise be due to the effects of the radiation acceleration on sodium atom orbits emitted near eastern elongation.

The motion of atoms in the elongated sodium cloud are somewhat parallel to the central cloud axis, illustrated in Figure 1, which is tilted toward Jupiter by 35°. The velocity of these atoms parallel to this axis is variable. For the simple case shown in Figure 1, the Sun-atom radial velocity v varies from a maximum value of about 22 km s^{-1} when the central axis is parallel to the Sun-Jupiter line to a minimum of zero (neglecting Jupiter's radial motion) when the central axis is perpendicular to the Sun-Jupiter line. This change in the velocity v with satellite phase angle clearly modulates the magnitude of the radiation acceleration b through the fraction $\gamma_i(v)$, while the vector direction of the acceleration is always fixed parallel to the Sun-Jupiter line.

A comparison of sodium atom orbits including and excluding the effect of the solar radiation acceleration will now be presented. The atom orbit defining the inner boundary (i.e., the one closest to Jupiter) of the sodium cloud shown in Figure 1 will be chosen as the unperturbed orbit (see Fig. 6 in Smyth and McElroy 1978). This orbit is calculated using the circular restricted three-body equations and determines the motion of a sodium atom in the combined gravitational fields of Io and Jupiter. The perturbed orbit is calculated by solving the circular restricted three-body equations of motion modified to include the complete effect of the solar radiation acceleration given by (4).

The initial conditions for the unperturbed and perturbed orbit calculations are identical. An atom is emitted radially from the inner trailing quadrant of the satellite's exosphere (assumed 2600 km in radius) with a speed of 2.6 km s^{-1}. The velocity vector is confined to the satellite plane and makes an angle of 70° with the Jupiter-Io line. The lifetime of the sodium atom is 20 hours.

In Figure 2 the unperturbed and perturbed atom orbits are compared for two different initial satellite phase angles, thereby illustrating the distortion that occurs in the inner cloud boundary observed both east and west of Jupiter. To exhibit this distortion appearing at an eastern phase angle of 55°, an atom orbit emitted initially at a satellite phase angle of 245° near western elongation is shown in Figure 2*a*. In this case, the solar radiation force acts in a direction to enhance either the angular or outward radial component of velocity of the emitted sodium atom over most of its 20 hour lifetime. This increases the kinetic energy of the atom and produces an orbit that remains more distant from Jupiter and that has a slightly larger period than the orbit calculated with zero radiation force. The atom orbit is therefore deflected less toward Jupiter than the unperturbed orbit, as illustrated in Figure 2*a*. In addition, the relative separation distance of the atom from Io at a given time is less than in the unperturbed orbit case since its larger period will be closer in value to the satellite period than will the unperturbed period. The first effect will cause the tilt angle of the perturbed central cloud axis to be less than 35° when the cloud is observed near a satellite phase angle of 55°. The second effect will cause the cloud to be compressed along its central cloud axis and hence have a larger density when observed near the 55° phase angle. These two effects are in the correct sense to explain the east-west asymmetries.

Figure 2*b* shows the distortion of the inner cloud boundary appearing at a western phase angle of 235°, for an atom orbit having originally been emitted at a satellite phase angle of 65°. The solar radiation force in this case acts in a direction to initially decrease the angular component and later to decrease the outward radial component of velocity of the emitted atom during its 20 hour lifetime. The initial energy loss and the later inward directed force will produce an orbit which lies closer to Jupiter and has a slightly smaller period than the orbit calculated with zero radiation force. The perturbed atom orbit in Figure 2*b* is therefore deflected more toward Jupiter and has a larger atom-Io separation distance for a given flight time than the unperturbed orbit. The perturbed central axis of the sodium cloud will therefore be tilted more than 35°. The perturbed cloud shape will be elongated along its central cloud axis with a corresponding decrease in the sodium density. Again, these two effects are in the correct sense to explain the east-west asymmetries. The two perturbed atom orbits of Figure 2 are compared directly with the unperturbed orbit in Figure 3.

To depict the overall distortion of the cloud shape at satellite phase angles of 55° and 235°, many such perturbed orbits must be calculated similar to the two shown in Figure 3. The location of these atoms on their orbits at 20 hours of flight time will then provide points from which an envelope for the cloud may be constructed. The orbits used to construct such an envelope in Figure 1 had initial conditions differing from the unperturbed orbit of Figure 3 only in the direction of the initial atom velocity vectors, which were allowed to range from −50° to +130° with respect to the Jupiter-Io line. Adopting this same set of initial conditions, the cloud envelopes for the perturbed orbits are calculated as they would appear at satellite phase angles of 55° and 235°. Results are

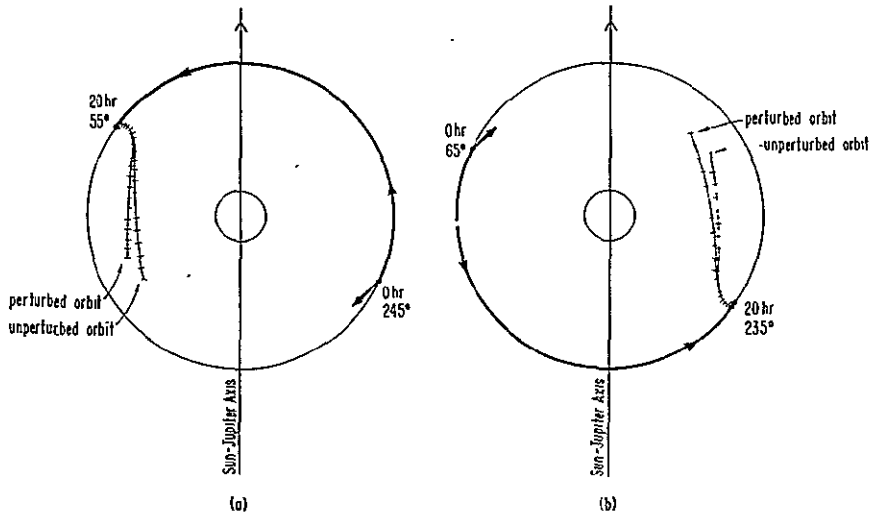

FIG. 2.—Perturbation of a sodium atom orbit by the solar radiation acceleration. The motion relative to Io of a perturbed atom orbit emitted by the satellite is compared with the motion of an unperturbed atom orbit for two different initial locations of the satellite. Tick marks occur at 1 hour intervals along the atom orbits. The initial atom velocity vector, Io's circular orbit about Jupiter, and the satellite motion during the 20 hour atom lifetime are shown relative to the Sun-Jupiter axis.

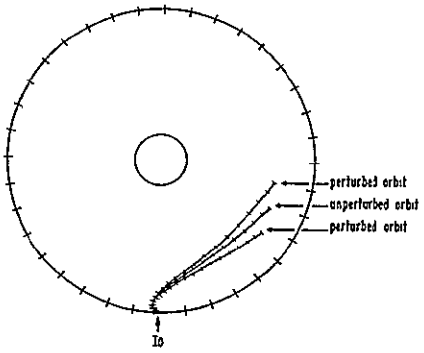

FIG. 3.—Comparison of the perturbed sodium atom orbits. The perturbed atom orbits shown in Fig. 2 at a phase angle of 55° and 235° are compared directed with each other and with the unperturbed atom orbit. Tick marks at 10° intervals along Io's circular orbit are indicated.

shown in Figure 4 and are compared with the unperturbed cloud envelope of Figure 1.

In Figure 4*a*, the sodium cloud shown at a phase angle of 55° appears to have a central axis tilted less than 35° toward Jupiter, as anticipated. The whole cloud also appears to be translated perpendicular to its central axis in a direction away from Jupiter. The forward portion of the cloud is shortened and less broad whereas the trailing portion of the cloud is elongated. The cloud is therefore compressed. The exact tilt angle of the central cloud axis, parallel to which the sodium appears nearly symmetrically distributed, will depend upon the distribution of sodium within the cloud envelope. Detailed three-dimensional density calculations are now in progress to establish this value. Examination of the shape of the envelope, however, suggests that the perturbed central axis may be tilted about 10° less than the unperturbed axis.

In Figure 4*b*, distortion of the sodium cloud envelope is shown for a phase angle of 235° (i.e., the symmetrically opposite phase angle situation to that shown in Fig. 4*a*). The perturbed cloud is tilted more toward Jupiter than the 35° angle of the unperturbed cloud, with perhaps a 5° increase suggested by the envelope shape. The forward extent of the cloud is elongated whereas the trailing portion of the cloud is less extended. The perturbed cloud is probably less dense because of the forward elongation, although the density change appears to be less pronounced than for the results of Figure 4*a*.

IV. CONCLUDING REMARKS

The distortion in the sodium cloud produced by the solar radiation acceleration associated with resonance scattering of atoms in the D_1 and D_2 lines, illustrated in Figure 4, offers a simple explanation for both east-west asymmetries. The solar radiation pressure acts in a time-dependent fashion, compressing the cloud near eastern elongation and expanding the cloud near western elongation, and provides an explanation for the east-west intensity asymmetry of Bergstralh *et al.* (1975, 1977). The solar radiation pressure also causes the cloud to tilt closer to Jupiter when Io is near western elongation than when Io is near eastern elongation, thereby providing an explanation for the east-west cloud distribution asymmetry of Goldberg *et al.* (1978).

The cloud envelopes in Figure 4 suggest an east-west change in the tilt angle of the central cloud axis of about 15°, although detailed three-dimensional orbit calculations, now in progress, are required to determine an exact value. The critical satellite phase angle, where an Earth observer sees the sodium distributed nearly symmetrically about Io, depends upon this tilt angle and also upon the Sun-Jupiter-Earth angle

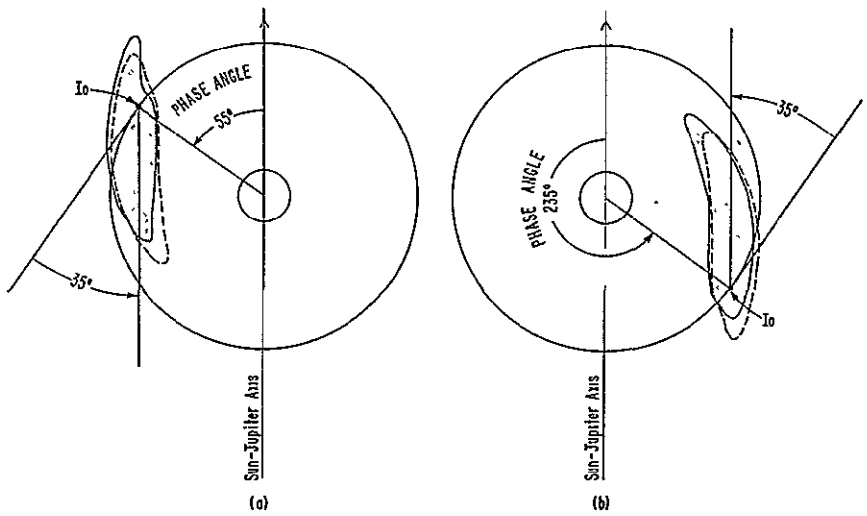

FIG. 4.—East-west changes in the sodium cloud. The change in the sodium cloud shape produced by the solar radiation acceleration is shown for two symmetrically opposite satellite phase angles. The perturbed cloud shape is indicated by the shaded area and is compared to the unperturbed cloud shape indicated by the dashed line.

which varies by about ±12°. The observed critical phase angles of 70°–75° in the east (Goldberg 1979) and 230° in the west (Goldberg *et al.* 1978) will include the effects of this latter angle.

The explanation presented for the east-west asymmetries of Io's sodium cloud clarifies and strengthens the idea advanced from earlier measurements of Bergstralh *et al.* (1975, 1977) that sodium atoms are emitted from the satellite at a constant rate. It also reinforces the modeling results of Matson *et al.* (1978) and Smyth and McElroy (1978) that sodium atoms are emitted nonisotropically from Io. These conclusions may be important in studying the global effects of active volcanoes (Morabito *et al.* 1979; Smith *et al.* 1979) and the intense satellite plasma torus (Broadfoot *et al.* 1979; Bridge *et al.* 1979; Warwick *et al.* 1979), both discovered recently for Io from *Voyager 1* spacecraft measurements. In this regard, future analysis of the east-west asymmetry data using three-dimensional models should be valuable. The apparent nonisotropic emission of sodium by the satellite might, for example, be due either to an asymmetry in the sodium supply and escape mechanism or to spatial asymmetries in the plasma properties responsible for ionizing the sodium cloud atoms. In either case, modeling of the sodium cloud data would provide a useful tool for Earth-based monitoring of these conditions over an extended period of time.

The author would like to thank R. Goody for helpful comments. This research was supported by the Planetary Atmospheres program of the National Aeronautics and Space Administration under grant NASW-3174.

REFERENCES

Allen, C. W. 1976, *Astrophysical Quantities* (London: Athlone).
Bergstralh, J. T., Matson, D. L., and Johnson, T. V. 1975, *Ap. J. (Letters)*, **195**, L131.
Bergstralh, J. T., Young, J. W., Matson, D. L., and Johnson, T. V. 1977, *Ap. J. (Letters)*, **211**, L51.
Bertaux, J. L., and Blamont, J. E. 1973, *J. Geophys. Res.*, **78**, 80.
Bridge, H. S., *et al.* 1979, *Science*, **204**, 987.
Broadfoot, A. L., *et al.* 1979, *Science*, **204**, 979.
Brown, R. A. 1974, in *IAU Symposium 65, Exploration of the Planetary System*, ed. A. Woszczyk and C. Iwaniszewska (Dordrecht: Reidel), pp. 527–531.
Brown, R. A., and Chaffee, F. H., Jr. 1974, *Ap. J. (Letters)*, **187**, L125.
Brown, R. A., Goody, R. M., Murcray, F. J., and Chaffee, F. H., Jr. 1975, *Ap. J. (Letters)*, **200**, L49.
Carlson, R. W., Matson, D. L., and Johnson, T. V. 1975, *Geophys. Res. Letters*, **2**, 469.
Carlson, R. W., Matson, D. L., Johnson, T. V., and Bergstralh, J. T. 1978, *Ap. J.*, **223**, 1082.
Finson, M. L., and Probstein, R. F. 1968, *Ap. J.*, **154**, 327.
Goldberg, B. A. 1979, private communication.
Goldberg, B. A., Carlson, R. W., Matson, D. L., and Johnson, T. V. 1978, *Bull. AAS*, **10**, 579.
Goody, R., and Apt, J. 1977, *Planet. Space Sci.*, **25**, 603.
Keller, H. U., and Thomas, G. E. 1975, *Astr. Ap.*, **39**, 7.
Kozai, Y. 1961, Smithsonian Ap. Obs. Spec. Rept., No. 56, pp. 25–33.
Macy, W. W., and Trafton, L. M. 1975, *Ap. J.*, **200**, 510.
Matson, D. L., Goldberg, B. A., Johnson, T. V., and Carlson, R. W. 1978, *Science*, **199**, 531.
Mekler, Yu., and Eviatar, A. 1974, *Ap. J. (Letters)*, **193**, L151.
———. 1978, *J. Geophys. Res.*, **83**, 5679.
Mekler, Yu., Eviatar, A., and Coroniti, F. V. 1976, *Ap. Space Sci.*, **40**, 63.
Morabito, L. A., Synnott, S. P., Kupferman, P. N., and Collins, S. A. 1979, *Science*, **204**, 972.
Münch, G., and Bergstralh, J. T. 1977, *Pub. A.S.P.*, **89**, 232.
Münch, G., Trauger, J., and Roesler, F. 1976, *Bull. AAS*, **8**, 468.
Murcray, F. J., and Goody, R. M. 1978, *Ap. J.*, **226**, 327.
Smith, B. A., *et al.* 1979, *Science*, **204**, 951.
Smyth, W. H., and McElroy, M. B. 1977, *Planet. Space Sci.*, **25**, 415.
———. 1978, *Ap. J.*, **226**, 336.
Trafton, L. 1975, *Ap. J. (Letters)*, **202**, L107.
———. 1977, *Ap. J.*, **215**, 960.
Trafton, L., and Macy, W., Jr. 1975, *Ap. J. (Letters)*, **202**, L155.
———. 1977, *Ap. J.*, **215**, 971.
Trafton, L., Parkinson, T., and Macy, W. 1974, *Ap. J. (Letters)*, **190**, L85.
Trauger, J., Roesler, F., and Münch, G. 1976, *Bull. AAS*, **8**, 468.
Warwick, J. W., *et al.* 1979, *Science*, **204**, 995.
Wehinger, P. A., Wyckoff, S., and Frolich, A. 1976, *Icarus*, **27**, 425.

WILLIAM H. SMYTH: Atmospheric and Environmental Research, Inc., 872 Massachusetts Avenue, Cambridge, MA 02139